Article

Neuron

Rostral and Caudal Ventral Tegmental Area GABAergic Inputs to Different Dorsal Raphe Neurons Participate in Opioid Dependence

Highlights

- Rostral and caudal VTA GABAergic neurons target different DRN neurons
- Rostral and caudal VTA→DRN pathways function oppositely in reward
- The rostral VTA→DRN pathway is depressed by repeated usage of morphine
- Chronically activating the rVTA→DRN inhibitory pathway disrupts morphine reward

Authors

Yue Li, Chun-Yue Li, Wang Xi, ..., Shumin Duan, Yu-Dong Zhou, Xiao-Ming Li

Correspondence

lixm@zju.edu.cn

In Brief

Li and Li et al. dissect the microcircuits between VTA GABAergic neurons and DRN neurons, identifying distinct pathways that specifically modulate morphine reward without affecting the analgesic effects of morphine.

Li et al., 2019, Neuron *101*, 1–14
February 20, 2019
https://doi.org/10.1016/j.neuron.2018.12.012

CellPress

Please cite this article in press as: Li et al., Rostral and Caudal Ventral Tegmental Area GABAergic Inputs to Different Dorsal Raphe Neurons Participate in Opioid Dependence, Neuron (2018), https://doi.org/10.1016/j.neuron.2018.12.012

Neuron
Article

Rostral and Caudal Ventral Tegmental Area GABAergic Inputs to Different Dorsal Raphe Neurons Participate in Opioid Dependence

Yue Li,[1,3] Chun-Yue Li,[1,3] Wang Xi,[1] Sen Jin,[2] Zuo-Hang Wu,[1] Ping Jiang,[1] Ping Dong,[1] Xiao-Bin He,[2] Fu-Qiang Xu,[2] Shumin Duan,[1] Yu-Dong Zhou,[1] and Xiao-Ming Li[1,4,*]

[1]Center for Neuroscience and Department of Neurology of Second Affiliated Hospital, NHC and CAMS Key Laboratory of Medical Neurobiology, Joint Institute for Genetics and Genome Medicine between Zhejiang University and University of Toronto, Zhejiang University School of Medicine, Hangzhou 310058, China

[2]CAS Center for Excellence in Brain Science, Chinese Academy of Sciences, Wuhan Institute of Physics and Mathematics, Wuhan 430071, China

[3]These authors contributed equally

[4]Lead Contact

*Correspondence: lixm@zju.edu.cn

https://doi.org/10.1016/j.neuron.2018.12.012

SUMMARY

Both the ventral tegmental area (VTA) and dorsal raphe nucleus (DRN) are involved in affective control and reward-related behaviors. Moreover, the neuronal activities of the VTA and DRN are modulated by opioids. However, the precise circuits from the VTA to DRN and how opioids modulate these circuits remain unknown. Here, we found that neurons projecting from the VTA to DRN are primarily GABAergic. Rostral VTA (rVTA) GABAergic neurons preferentially innervate DRN GABAergic neurons, thus disinhibiting DRN serotonergic neurons. Optogenetic activation of this circuit induces aversion. In contrast, caudal VTA (cVTA) GABAergic neurons mainly target DRN serotonergic neurons, and activation of this circuit promotes reward. Importantly, μ-opioid receptors (MOPs) are selectively expressed at rVTA→DRN GABAergic synapses, and morphine depresses the synaptic transmission. Chronically elevating the activity of the rVTA→DRN pathway specifically interrupts morphine-induced conditioned place preference. This opioid-modulated inhibitory circuit may yield insights into morphine reward and dependence pathogenesis.

INTRODUCTION

The dorsal raphe nucleus (DRN) is a well-organized hindbrain structure containing half of brain total serotonergic neurons (Jacobs and Azmitia, 1992). DRN serotonergic neurons are involved in affective control (Dayan and Huys, 2009); however, the role of serotonin in reward-related behaviors is still controversial. Recent research has shown that activation of DRN serotonergic neurons is reinforcing (Li et al., 2016; Liu et al., 2014), whereas other studies indicate that DRN serotonergic neurons are activated by both reward and punishment (Cohen et al., 2015; Ren et al., 2018). Such differences may be explained by the existence of subpopulations of DRN serotonergic neurons and/or circuits related to the DRN.

It is widely accepted that the ventral tegmental area (VTA) plays an important role in the control of motivated behaviors (Bromberg-Martin et al., 2010). Interaction between the VTA and DRN is of long-standing interest and may be of great importance for discovering the role of the DRN in reward and aversion. According to previous study, DRN serotonergic neurons strongly innervate the VTA (Watabe-Uchida et al., 2012). However, the characteristics and functions of the circuits projecting from the VTA to DRN remain unclear (Ogawa et al., 2014; Pollak Dorocic et al., 2014; Weissbourd et al., 2014). To further understand the controversial results regarding the role of serotonin in reward-related behaviors in the DRN, it is critical to dissect the architecture and function of the subcircuits between the VTA and DRN and study how they are differentially regulated.

The VTA is the main target of multiple addictive drugs, including opioids, psychostimulants, and cannabinoids (Lüscher and Malenka, 2011). Interestingly, opioids specifically target and inhibit VTA GABAergic neurons through μ-opioid receptors (MOPs), leading to the disinhibition of VTA dopaminergic neurons (Fields and Margolis, 2015; Johnson and North, 1992). However, how opioids modulate VTA projection GABAergic neurons remains unclear. Intriguingly, GABAergic transmissions in serotonergic neurons in the DRN increase under chronic morphine administration, resulting in a decrease in serotonin efflux (Jolas et al., 2000). Thus, we wondered whether VTA-DRN circuits could be modulated by opioids.

In the current study, we found that VTA projections in the DRN were mainly GABAergic, not dopaminergic. Unexpectedly, the rostral VTA (rVTA) preferentially innervated DRN GABAergic neurons, whereas the caudal VTA (cVTA) tended to target DRN serotonergic neurons. Second, rVTA and cVTA GABAergic projections in the DRN exhibited opposite functions in reward-related behaviors, probably by contrasting regulation of DRN serotonergic neuronal activity. Third, MOPs were differentially distributed in the rostral and caudal VTA GABAergic neuronal

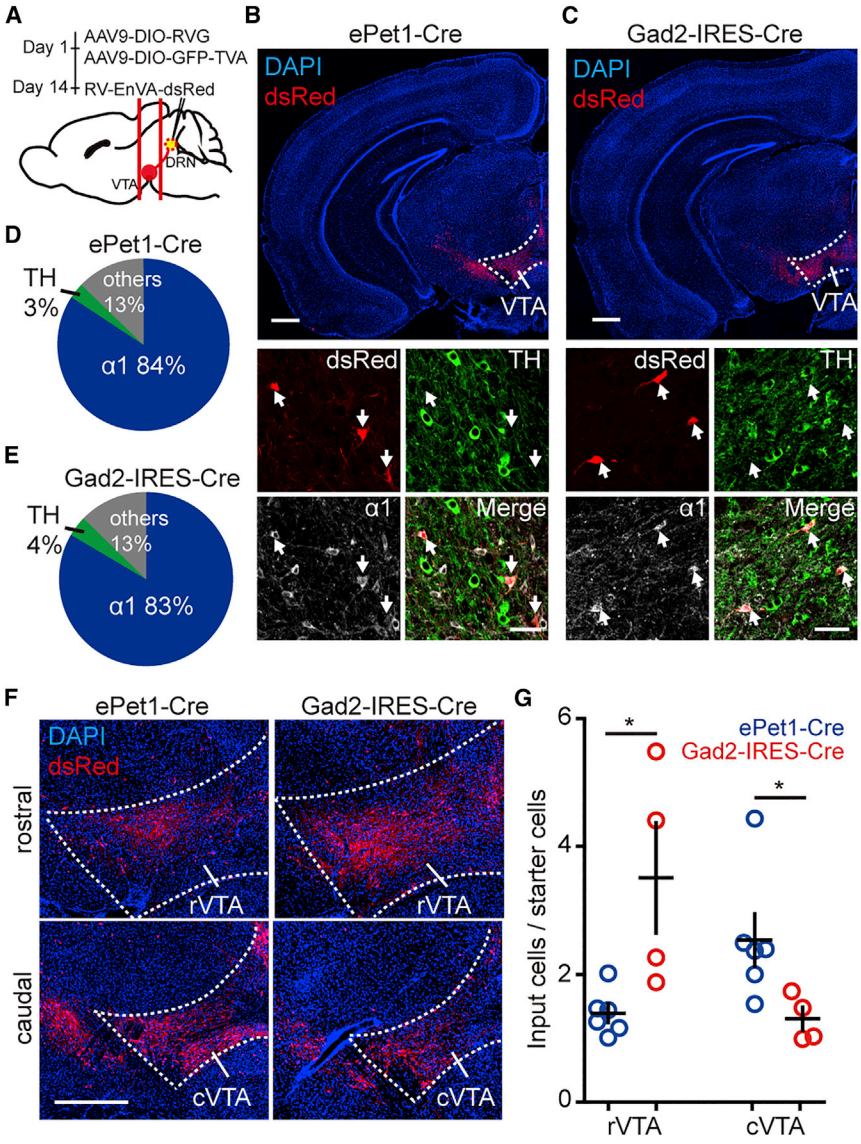

Figure 1. DRN Serotonergic and GABAergic Neurons Received Dense Projections from Caudal and Rostral VTA GABAergic Neurons

(A) Diagram of the virus injection protocol and injection site. Red lines represent section sites in the rostral and caudal VTA.

(B and C) Top: midbrain input cells (red) innervating DRN serotonergic (B) and GABAergic neurons (C). Bottom: input cells (red) to DRN serotonergic (B) and GABAergic neurons (C) mostly colocalized with $GABA_AR$ α1 (gray), but not TH (green).

(D and E) Pie charts represent the fraction of different cell types projecting from the VTA to DRN serotonergic (D) and GABAergic neurons (E) (n = 3 mice for each group).

(F) Representative input cells projecting from the rostral (top) and caudal (bottom) VTA to DRN serotonergic (left) and GABAergic (right) neurons.

(G) Input/starter ratio of ePet1-Cre and Gad2-IRES-Cre mice in the rostral VTA (ePet1-Cre, 1.392 ± 0.1433; Gad2-IRES-Cre, 3.505 ± 0.8637; p = 0.019; *U* = 1.0; Mann-Whitney test) and caudal VTA (ePet1-Cre, 2.538 ± 0.4072; Gad2-IRES-Cre, 1.305 ± 0.1810; p = 0.019; *U* = 1.0; Mann-Whitney test) (n = 6 and 4 for ePet1-Cre and Gad2-IRES-Cre mice, respectively).

Scale bars represent 500 μm (B and C, top panel, and F) and 50 μm (B and C, bottom panel). *p < 0.05. Error bars represent SEM. cVTA, caudal VTA; rVTA, rostral VTA.

See also Figures S1 and S2.

terminals within the DRN, resulting in different modulation of these two circuits by chronic morphine exposure. Finally, chronically elevating the activity of the rVTA→DRN inhibitory pathway during morphine administration interrupted morphine reward.

RESULTS

Neurons Projecting from the VTA to DRN Are Primarily GABAergic

To investigate the monosynaptic inputs from the VTA to DRN serotonergic and GABAergic neurons, we injected a mixture of helper viruses (AAV9-CAG-DIO-RVG and AAV9-CAG-DIO-GFP-TVA, 1:1) into the DRN of ePet1-Cre and Gad2-IRES-Cre mice followed by EnvA-pseudotyped and rabies virus glycoprotein (RVG)-deleted rabies virus RV-EnvA-dsRed at the same coordinates 2 weeks later (Figure 1A; Method Details). Only neurons expressing both the RVG and EnvA cognate receptor TVA (starter cells) allowed the retrograde spreading of the rabies virus to presynaptic neurons (input cells) (Wickersham et al., 2007).

Starter cells were co-stained with the serotonin marker tryptophan hydroxylase 2 (Tph2) to confirm the specificity of the virus. We found 91.9% ± 3.0% of the starter cells in ePet1-Cre mice were Tph2 positive (Figures S1A, S1B, and S1E), with no overlap observed between Tph2-positive and starter cells in Gad2-IRES-Cre mice (Figures S1C–S1E). Starter cells in a series of coronal sections matched the expression patterns of DRN serotonergic and GABAergic neurons (Weissbourd et al., 2014) (Figures S1F and S1G). Control experiments confirmed that the rabies-mediated transsynaptic tracing system was dependent on Cre and RVG expression (Figures S1I–S1L; Method Details).

In the midbrain, input cells were concentrated in the VTA, and both DRN serotonergic and GABAergic neurons received dense projections from the VTA (Figures 1B and 1C, top panel). Immunohistochemical analysis was performed to identify types of input cells in the VTA. As the $GABA_A$ receptor ($GABA_AR$) α1 subunit ($GABA_AR$ α1) is selectively clustered on VTA GABAergic neurons (Tan et al., 2010), we stained sections with $GABA_AR$ α1 and tyrosine hydroxylase (TH) antibodies to label VTA GABAergic and dopaminergic neurons (Figures 1B and 1C, bottom panel). Very few VTA afferents to the DRN were TH positive

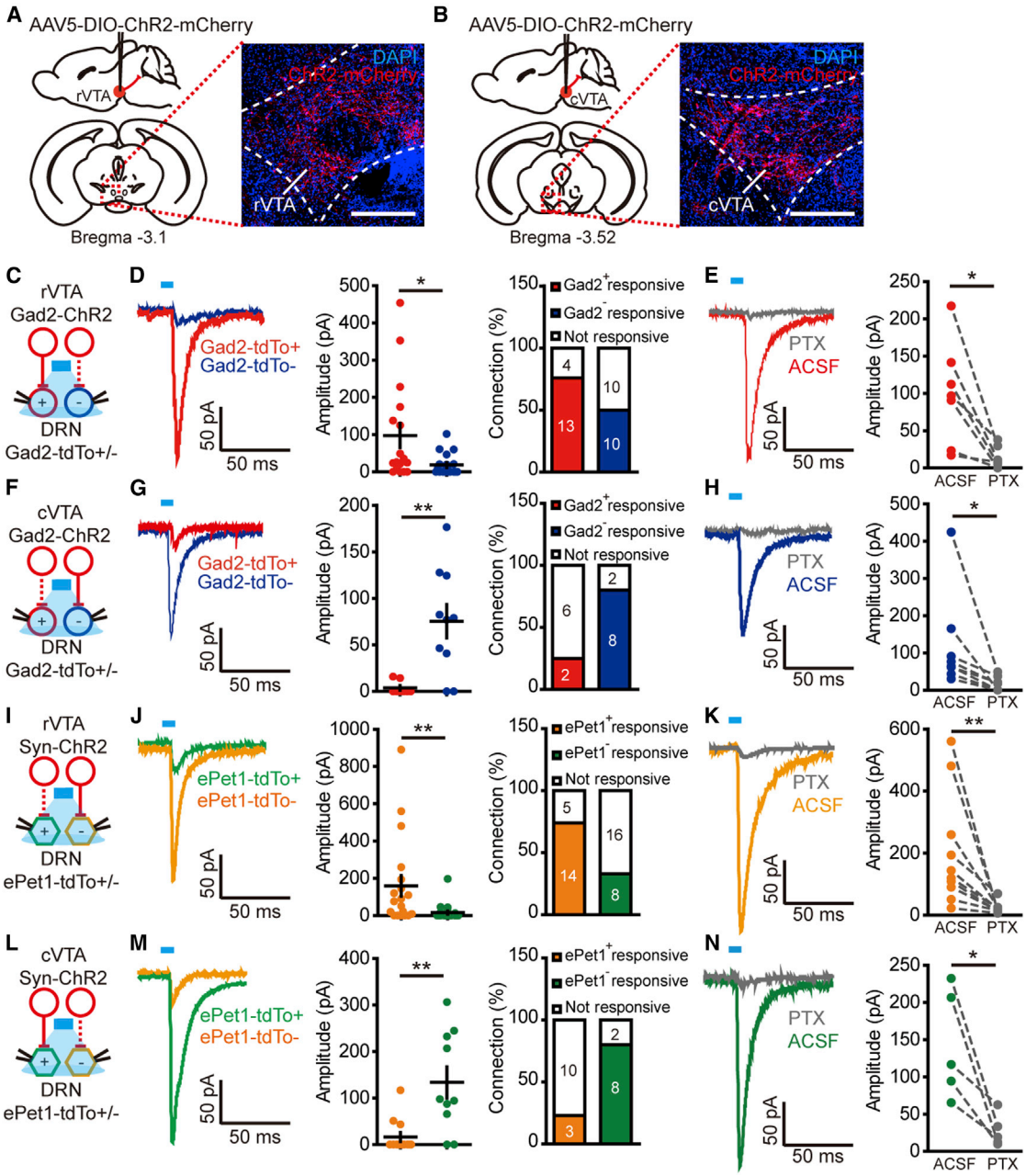

Figure 2. Rostral and Caudal VTA GABAergic Neurons Targeted DRN GABAergic and Serotonergic Neurons, Respectively

(A and B) Diagram of virus injection sites (left) and expression of ChR2-mCherry (red) (right) in the rVTA (A) and cVTA (B).

(C, F, I, and L) Schematics of recordings in the DRN Gad2-tdTomato-positive or negative neurons (C and F) and ePet1-tdTomato-positive or negative neurons (I and L) during photoactivation of ChR2 expressed in rVTA (C and I) or cVTA (F and L) terminals.

(D and G) Representative traces (left), amplitudes (middle), and number of connections (right) of eIPSCs recorded in GABAergic and non-GABAergic neurons during activation of rostral (D) (amplitude = 97.66 ± 32.73 pA and 18.41 ± 6.26 pA, connections = 76.5% and 50%, n = 17 and 20 neurons from 4 mice for GABAergic and non-GABAergic neurons, respectively; p = 0.016; U = 93; Mann-Whitney test) or caudal (G) (amplitude = 3.78 ± 2.48 pA and 75.44 ± 17.91 pA, connections = 25% and 80%, n = 8 and 10 neurons from 4 mice for GABAergic and non-GABAergic neurons, respectively; p = 0.006; U = 10; Mann-Whitney test) ChR2-expressing VTA terminals in the DRN.

(E and H) eIPSCs in rVTA→DRN pathway (E) (amplitude = 99.87 ± 26.07 pA and 13.11 ± 5.63 pA before and after application of PTX, respectively; n = 7 neurons from 6 mice; p = 0.0104; $t_{(6)}$ = 3.67; paired t test) or cVTA→DRN pathway (H) (amplitude = 119.6 ± 45.92 pA and 15.64 ± 6.818 pA before and after application of PTX, respectively; n = 8 neurons from 4 mice; p = 0.041; $t_{(7)}$ = 2.50; paired t test) blocked by PTX.

(J and M) Representative traces (left), amplitudes (middle), and connectivities (right) of eIPSCs recorded in serotonergic and non-serotonergic neurons during photoactivation of rostral (J) (amplitude 159.3 ± 54.77 pA and 15.28 ± 8.37 pA, connections = 73.7% and 33.3%, n = 19 and 24 neurons from 5 mice for non-serotonergic and serotonergic neurons, respectively; p = 0.0011; U = 102; Mann-Whitney test) or caudal (M) (amplitude 16.24 ± 9.7 pA and 133.5 ± 33.76 pA,

(legend continued on next page)

(Figures 1D and 1E). In contrast, the VTA inputs to DRN serotonergic and GABAergic neurons were mainly $GABA_AR$ α1 positive and TH negative (Figures 1D and 1E), indicating that these neurons were mainly GABAergic. Thus, these data suggest that the VTA sent strong GABAergic afferents to both serotonergic and GABAergic neurons in the DRN.

Rostral and Caudal VTA GABAergic Neurons Target Different DRN Neurons

The VTA is a large heterogeneous area divided into rostral and caudal parts (Sanchez-Catalan et al., 2014). We sectioned the VTA from rostral to caudal regions after the rabies virus injection to determine whether the distribution patterns of input cells between the rostral and caudal VTA were different (Figure 1A). The number of input cells was divided by the number of starter cells, and the ratios in the rVTA and cVTA were separately compared between the two mouse lines. In the rVTA, the input/starter ratio was higher in Gad2-IRES-Cre mice (Figures 1F, 1G, S1H, and S2). In contrast, the input/starter ratio was higher in the cVTA in ePet1-Cre mice (Figures 1F, 1G, S1H, and S2). Thus, the rVTA may send more projections to DRN GABAergic neurons, whereas the cVTA may innervate more serotonergic neurons in the DRN.

To confirm this connectivity pattern, we injected AAV5-ef1α-DIO-ChR2-mCherry into the rostral or caudal (R-C) VTA in Gad2-IRES-Cre mice to separately express channelrhodopsin-2 (ChR2) in rVTA (Figure 2A) or cVTA (Figure 2B) GABAergic neurons and performed electrophysiology to record light-evoked inhibitory postsynaptic currents (eIPSCs) on DRN slices. Immunohistochemistry were performed to confirm the specificity of ChR2 expression (Figures S3A–S3D). *In vitro* whole-cell recordings (Figure S3E) and *in vivo* local field potential (LFP) recordings (Figure S3G) were performed to confirm the effectiveness of ChR2. In addition, dense ChR2-mCherry-positive signals were observed in the DRN (Figure S3H), and photoactivation of cVTA GABAergic terminals in the DRN induced local neuronal responses (Figure S3I), further suggesting that the VTA sends GABAergic afferents to the DRN.

Gad2-IRES-Cre mice were crossed with Ai9 mice to label GABAergic neurons with tdTomato. 4–6 weeks after injecting AAV5-ef1α-DIO-ChR2-mCherry into the R-C VTA, slices containing the DRN were subjected to *in vitro* electrophysiology. When rVTA GABAergic terminals in the DRN were photoactivated (Figure 2C), eIPSCs with larger amplitudes and a greater number of connections were recorded in DRN GABAergic neurons than in non-GABAergic neurons (Figure 2D). The eIPSCs were inhibited by the $GABA_AR$ antagonist picrotoxin (PTX), indicating that $GABA_AR$ mediated neurotransmission (Figure 2E). Biocytin staining showed that the recorded putative GABAergic neurons were all co-localized with tdTomato (Figures S3J and S3L). In contrast, when expressing ChR2 in cVTA GABAergic neurons (Figure 2F), eIPSCs recorded in DRN non-GABAergic neurons had larger amplitudes and a greater number of connections (Figure 2G). PTX inhibited the eIPSCs, indicating that $GABA_AR$ mediated neurotransmission (Figure 2H). From biocytin staining, 82% of the recorded non-GABAergic neurons were Tph2 positive (Figures S3K and S3L), indicating that they were serotonergic neurons. Light-evoked IPSCs recorded in the R-C VTA→DRN circuits were blocked by tetrodotoxin (TTX) but rescued by 4-aminopyridine (4-AP) (Figures S3M and S3N), indicating that R-C VTA GABAergic neurons monosynaptically inhibited DRN cells. It has been reported that VTA GABAergic neurons co-release glycine (Polter et al., 2018). Therefore, we bath applied the glycine receptor blocker strychnine to test whether it could attenuate the eIPSCs in the R-C VTA→DRN pathways. Bath application of bicuculline, but not strychnine, blocked the eIPSCs in both pathways (Figures S3O and S3P), indicating that the neural transmissions were mediated by GABA rather than by glycine.

To further confirm that the cVTA-targeted non-GABAergic neurons were serotonergic, we crossed ePet1-Cre mice with Ai9 mice to label serotonergic neurons with tdTomato and injected AAV5-Syn-ChR2-mCherry into the R-C VTA. Excitatory neurotransmission was blocked by bath application of α-amino-3-hydroxy-5-methyl-4-isoxazolepropionic acid (AMPA) receptor antagonist 6,7-dinitroquinoxaline-2,3-dione (DNQX). In agreement with previous results, eIPSCs with larger amplitudes and a greater number of connections were recorded in non-serotonergic neurons when the rVTA terminals in the DRN were photoactivated (Figures 2I and 2J); photoactivation of the cVTA terminals evoked IPSCs with larger amplitudes and a greater number of connections in the DRN serotonergic neurons (Figures 2L and 2M). PTX blocked the eIPSCs recorded in both serotonergic and non-serotonergic neurons in the DRN (Figures 2K and 2N).

These data provide strong evidence that the rVTA targets and exerts inhibitory effects on DRN GABAergic neurons, whereas the cVTA mainly innervates and inhibits DRN serotonergic neurons.

Rostral VTA GABAergic Neurons Disinhibit DRN Serotonergic Neurons by Inhibiting Local GABAergic Neurons in the DRN

We next recorded the firing rates of DRN GABAergic and non-GABAergic neurons during photoactivation of R-C VTA ChR2-expressing GABAergic terminals in slices containing the DRN to evaluate the effects of R-C VTA GABAergic projections on DRN neuronal activity.

Membrane potentials were held at −45 mV to induce action potentials, with the firing rates of DRN GABAergic and

connections = 23.1% and 80%, n = 13 and 10 neurons from 3 mice for non-serotonergic and serotonergic neurons, respectively; p = 0.003; $U = 20$; Mann-Whitney test) ChR2-expressing VTA terminals in the DRN.

(K and N) eIPSCs in rVTA→DRN pathway (K) (amplitude = 228.4 ± 57.65 pA and 21.21 ± 5.08 pA before and after application of PTX, respectively; n = 11 neurons from 5 mice; p = 0.005; $t_{(10)} = 3.58$; paired t test) or cVTA→DRN pathway (N) (amplitude = 143.2 ± 32.51 pA and 27.5 ± 9.715 pA before and after application of PTX, respectively; n = 5 neurons from 3 mice; p = 0.03; $t_{(4)} = 3.43$; paired t test) blocked by PTX.

Scale bars represent 300 μm (A and B). *p < 0.05, **p < 0.01. Error bars represent SEM.

See also Figure S3.

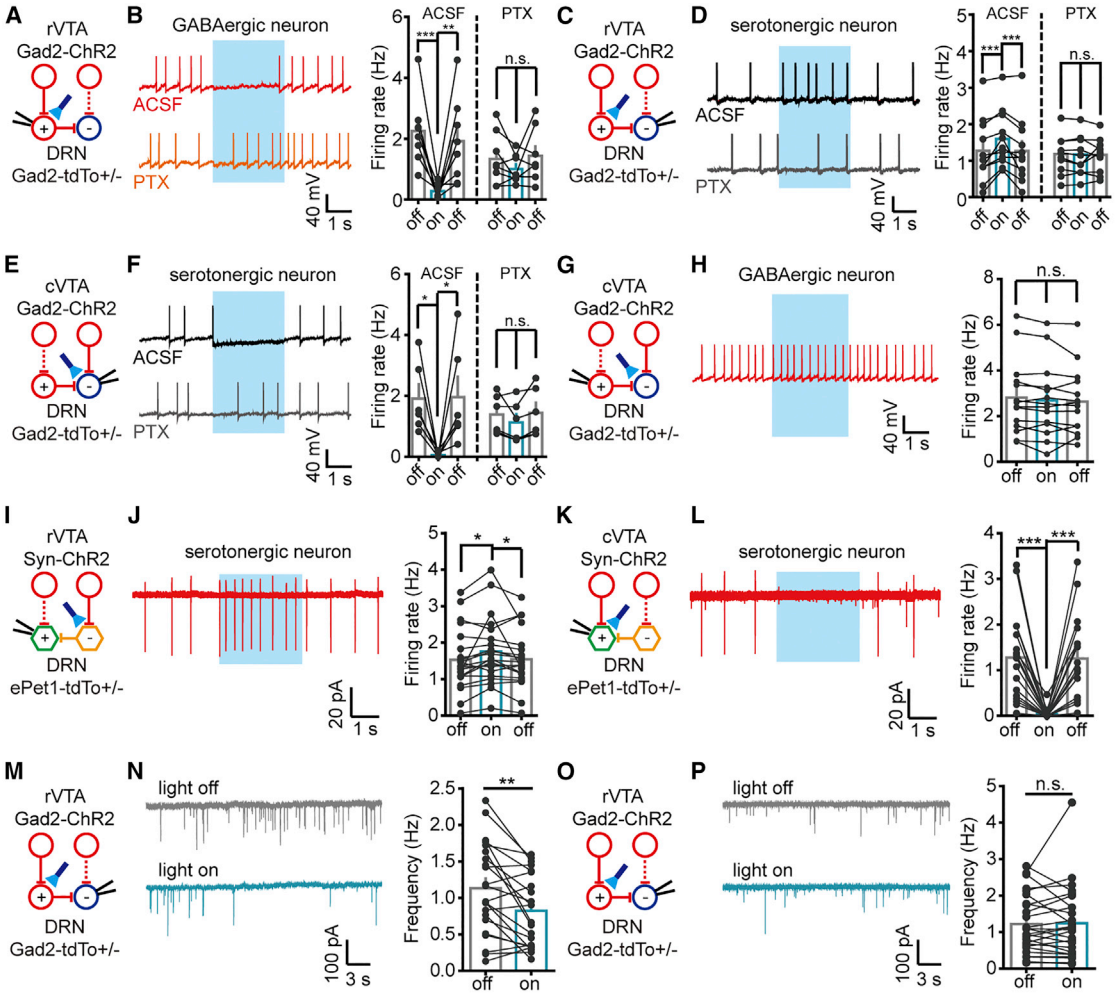

Figure 3. Photoactivation of rVTA→DRN GABAergic Inputs Disinhibited DRN Serotonergic Neurons via Direct Inhibition of DRN GABAergic Neurons

(A, C, E, G, I, K, M, and O) Schematics of recordings in DRN Gad2-tdTomato-positive (A and G) or negative (C, E, M, and O) neurons and ePet1-tdTomato-positive (I) or -negative (K) neurons during photoactivation of ChR2 expressed in the rVTA (A, C, I, M, and O) or cVTA (E, G, and K) terminals.

(B and D) Sample traces (left) and bar plots (right) showing firing rates of DRN GABAergic (B) (n = 8 neurons from 3 mice; for the artificial cerebrospinal fluid (ACSF) group, firing rates = 2.252 ± 0.4, 0.278 ± 0.08, and 1.918 ± 0.5 Hz before, during, and after photostimulation, respectively; $F_{2,14} = 14.49$, p = 0.0004, repeated one-way ANOVA with Tukey's post hoc test; for the PTX group, firing rates = 1.338 ± 0.3, 1.002 ± 0.16, and 1.437 ± 0.3 Hz before, during, and after photostimulation, respectively; $F_{2,14} = 1.848$, p = 0.194, repeated one-way ANOVA with Tukey's post hoc test) or serotonergic neurons (D) (n = 11 neurons from 4 mice; for the ACSF group, firing rates = 1.268 ± 0.27, 1.596 ± 0.24, and 1.265 ± 0.27 Hz before, during, and after photostimulation, respectively; $F_{2,20} = 14.35$, p = 0.0001, repeated one-way ANOVA, Tukey's post hoc test; for the PTX group, firing rates = 1.181 ± 0.16, 1.17 ± 0.16, and 1.161 ± 0.14 Hz before, during, and after photostimulation, respectively; $F_{2,20} = 0.06$, p = 0. 9418, repeated one-way ANOVA with Tukey's post hoc test) before, during, and after photoactivation of rVTA→DRN GABAergic inputs with or without PTX.

(F) Sample traces (left) and bar plots (right) showing firing rates of DRN serotonergic neurons (n = 6 neurons from 3 mice; for the ACSF group, firing rates = 1.91 ± 0.47, 0.06 ± 0.04, and 1.96 ± 0.67 Hz before, during, and after photostimulation, respectively; $F_{2,10} = 7.62$, p = 0.0098, repeated one-way ANOVA, Tukey's post hoc test; for the PTX group, firing rates = 1.39 ± 0.26, 1.12 ± 0.27, and 1.45 ± 0.33 Hz before, during, and after photostimulation, respectively; $F_{2,10} = 1.92$, p = 0.20, repeated one-way ANOVA with Tukey's post hoc test) before, during, and after photoactivation of cVTA→DRN GABAergic inputs with or without PTX.

(H) Sample traces (left) and bar plots (right) showing the firing rates of DRN GABAergic neurons (firing rates = 2.808 ± 0.44, 2.686 ± 0.43, and 2.635 ± 0.39 Hz before, during, and after photostimulation, respectively; n = 14 neurons from 3 mice; $F_{2,26} = 2.19$, p = 0.13, repeated one-way ANOVA with Tukey's post hoc test) before, during, and after the photoactivation of cVTA→DRN GABAergic inputs.

(J and L) Sample traces (left) and bar plots (right) showing firing rates of DRN serotonergic neurons before, during, and after photoactivation of rostral (J) (firing rates = 1.528 ± 0.18, 1.759 ±± 0.2, and 1.542 ± 0.17 Hz before, during, and after photostimulation, respectively; n = 21 neurons from 3 mice; $F_{2,40} = 5.179$, p = 0.01, repeated one-way ANOVA with Tukey's post hoc test) or caudal (L) (firing rates = 1.273 ± 0.23, 0.036 ± 0.03, and 1.254 ± 0.22 Hz before, during, and after photostimulation, respectively; n = 17 neurons from 3 mice; $F_{2,32} = 28.62$, p < 0.0001, repeated one-way ANOVA with Tukey's post hoc test) VTA→DRN GABAergic inputs.

(legend continued on next page)

non-GABAergic neurons then recorded before, during, and after photostimulation. Light significantly inhibited the firing rates of GABAergic neurons when rVTA GABAergic terminals were photoactivated (Figures 3A and 3B). This inhibition was diminished by PTX application (Figure 3B), further confirming that DRN GABAergic neurons received direct inhibition from rVTA GABAergic neurons. In contrast, the firing rates of biocytin-identified serotonergic neurons were increased when rVTA GABAergic terminals were photoactivated (Figures 3C and 3D). Based on this result, together with the finding that DRN serotonergic neurons were inhibited by local GABAergic neurons (Huang et al., 2017) (Figures S4A–S4C), we hypothesized that activation of rVTA GABAergic neurons could disinhibit DRN serotonergic neurons by directly inhibiting local GABAergic interneurons. The disinhibition model was further supported by blockade of the increase in firing rates by PTX (Figure 3D). When cVTA GABAergic terminals in the DRN were photoactivated, the firing rates of biocytin-identified serotonergic neurons were reduced by light (Figures 3E and 3F) and the reduction could be blocked by PTX (Figure 3F), indicating $GABA_AR$-mediated inhibition. No effect was observed on GABAergic neurons when the cVTA→DRN circuit was photoactivated (Figures 3G and 3H). Thus, the cVTA mainly inhibited DRN serotonergic neurons, in agreement with the results shown in Figures 2G and 2M.

The spontaneous activity of serotonergic neurons in the DRN is driven by the norepinephrine system *in vitro* (Vandermaelen and Aghajanian, 1983). We restored the spontaneous firing of DRN serotonergic neurons by adding DL-norepinephrine hydrochloride (NE) (30 μM) to the recording buffer and recorded the spontaneous firing rates of DRN ePet1-tdTomato-positive neurons in cell-attached mode while photoactivating R-C VTA GABAergic inputs (Figures 3I and 3K). Consistent with our results in Figures 3D and 3F, the firing rates of DRN serotonergic neurons were increased by activation of rVTA GABAergic inputs (Figure 3J) but were inhibited by activation of cVTA GABAergic innervations (Figure 3L). This indicates that the rVTA and cVTA oppositely regulated serotonergic neuronal activities in the DRN.

To further test the hypothesis that rVTA GABAergic neurons disinhibited DRN serotonergic neurons, we recorded spontaneous IPSCs (sIPSCs) in DRN non-GABAergic neurons before and during photoactivation of inhibitory inputs from the rVTA (Figure 3M). The frequencies of sIPSCs recorded in DRN non-GABAergic neurons were significantly decreased after 30 s of 20-Hz blue light illumination (Figure 3N). Based on this result, the inhibitory inputs to DRN non-GABAergic neurons were diminished when most DRN GABAergic neurons were inhibited by rVTA GABAergic neurons. The frequency of miniature IPSCs (mIPSCs) was not altered by light, indicating that the decrease in sIPSC frequency was activity dependent (Figures 3O and 3P).

To study the local circuits in the DRN, we expressed ChR2 in DRN GABAergic and serotonergic neurons. Light-evoked IPSCs were recorded in non-GABAergic neurons when photoactivating ChR2-expressing DRN GABAergic neurons (Figure S4A). All neurons recorded eIPSCs in the presence of TTX and 4-AP, and eIPSCs could be blocked by PTX (Figures S4B and S4C). When expressing ChR2 in DRN serotonergic neurons (Figure S4D), we could not record any eEPSCs, eIPSCs, or mixed responses following a 5-ms single pulse (Figure S4E). Serotonin-mediated postsynaptic potentials following 5 s of 20-Hz light illumination were not detected either (Figure S4F). These results indicate that DRN GABAergic neurons inhibited serotonergic neurons directly, but serotonergic neurons may not influence local GABAergic neurons directly.

Rostral and Caudal VTA Inhibitory Inputs to the DRN Have Opposite Functions in Reward-Related Behaviors

VTA GABAergic neurons participate in reward-related behaviors by inhibiting local dopaminergic neurons (Tan et al., 2012; van Zessen et al., 2012) or projecting to other brain areas that control motivated behaviors (Root et al., 2014; Stamatakis et al., 2013). The DRN is also involved in affective control (Dayan and Huys, 2009; Liu et al., 2014). Therefore, we hypothesized that modulation of the VTA→DRN circuit would result in a reward-related phenotype. To test this hypothesis, we expressed ChR2 or *N. pharaonis* halorhodopsin (NpHR) in R-C VTA GABAergic neurons (Figures 2A, 2B, S3F, and S5), with optical fibers implanted above the DRN to allow light-mediated activation or inhibition of R-C VTA inhibitory inputs in the DRN (Figures 4A and 4G). We used real-time place preference (RTPP) or aversion (RTPA) paradigms (see Method Details). The mice, as compared with littermate controls, showed avoidance of the chamber receiving photoactivation of rVTA→DRN inhibitory inputs (Figures 4B and 4C). The inhibition of this circuit elicited a preference for the photostimulation-paired chamber (Figures 4B and 4D). In contrast to the rVTA, activation of cVTA→DRN inhibitory inputs resulted in a preference for the photostimulation-paired chamber (Figures 4H and 4I), and the inhibition of this circuit resulted in avoidance of the photostimulation-paired chamber (Figures 4H and 4J). Activation of neural terminals might induce backpropagating action potentials in the soma. Thus, the behavior changes may be due to activation of VTA GABAergic neurons and inhibition of dopaminergic neurons. To test this, we microinjected PTX into the DRN through a guide cannula. Microinjecting PTX into the DRN blocked the avoidance or preference for the photostimulation-paired chamber (Figures 4E, 4F, 4K, and 4L), indicating that this behavioral outcome was dependent on $GABA_AR$ within the DRN but was not due to activation of pass-by fibers or cell bodies retrogradely. These behaviors were not due to the

(N) Representative traces (left) and bar plots (right) of sIPSCs recorded in DRN non-GABAergic neurons before and during photostimulation of rVTA→DRN GABAergic inputs (frequency = 1.132 ± 0.133 and 0.8243 ± 0.105 Hz before and during photostimulation, respectively; n = 22 neurons from 3 mice; p = 0.0013; $t_{(21)}$ = 3.71; paired t test).

(P) Representative traces (left) and bar plots (right) of mIPSCs recorded in DRN non-GABAergic neurons before and during photostimulation of rVTA→DRN GABAergic inputs (frequency = 1.221 ± 0.16 and 1.244 ± 0.19 Hz before and during photostimulation, respectively; n = 26 neurons from 3 mice; p = 0.82; $t_{(25)}$ = 0.23; paired t test).

*p < 0.05, **p < 0.01, ***p < 0.001; n.s., no significant difference. Error bars represent SEM.

See also Figure S4.

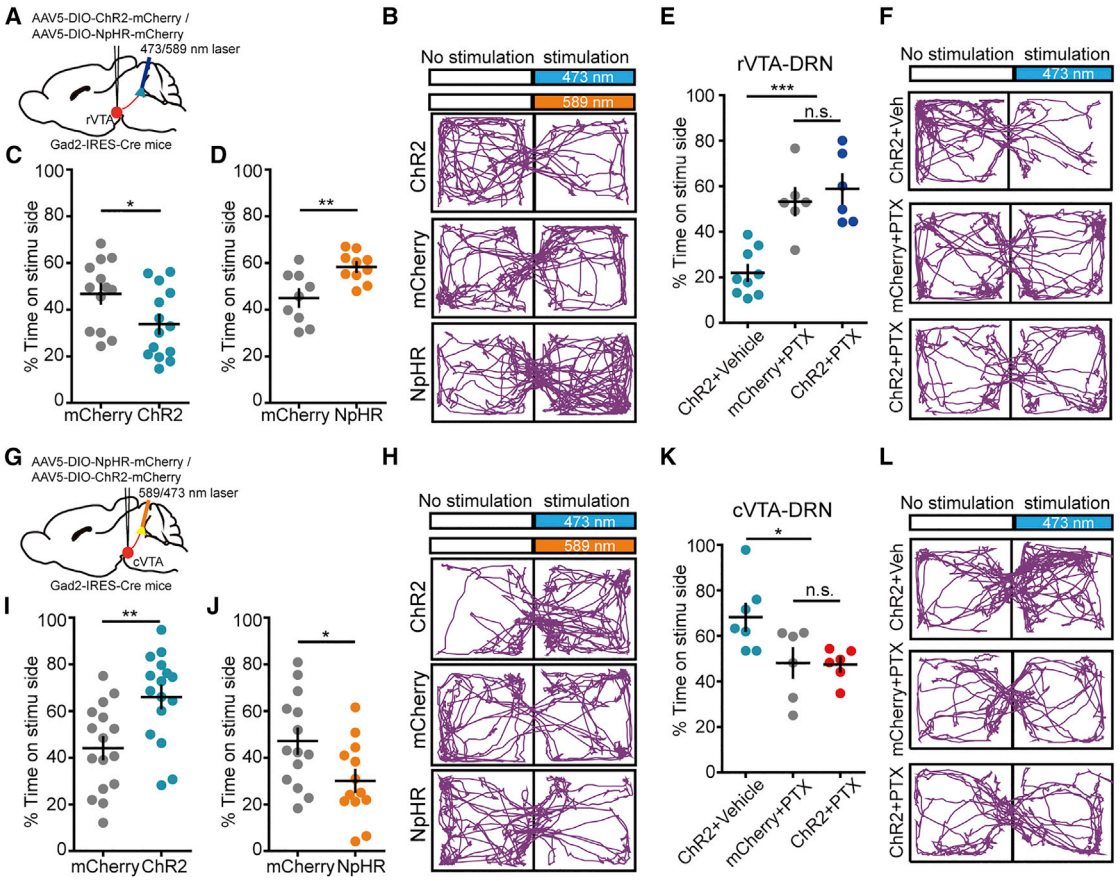

Figure 4. R-C VTA Inhibitory Inputs to the DRN Have Opposite Functions in Real-Time Place Preference

(A and G) Diagrams of virus injection sites in rostral (A) or caudal (G) VTA and photostimulation sites in the DRN.

(B, F, H, and L) Tracking data showing the locus in the RTPP arena of mice expressing ChR2-mCherry, mCherry, or NpHR-mCherry in the rVTA (B and F) or cVTA (H and L).

(C and D) Percentage of time spent in photoactivation-paired (C) (ChR2 group, 33.79% ± 3.95%; mCherry group, 46.79% ± 4.05%; n = 14 and 13 mice for ChR2 and mCherry groups, respectively; p = 0.03; $t_{(25)}$ = 2.30; two-tailed t test) or photoinhibition-paired (D) (NpHR group, 58.25% ± 2.02%; mCherry group, 44.96% ± 3.68%; n = 10 and 9 mice for NpHR and mCherry groups, respectively; p = 0.005; $t_{(17)}$ = 3.26; two-tailed t test) chamber when opsins were expressed in rVTA GABAergic neurons.

(E) Preference for the chamber paired with rVTA→DRN inhibitory circuit photoactivation was inhibited by microinjection of PTX into the DRN (ChR2 + vehicle group, 21.94% ± 3.37%, n = 9 mice; mCherry + PTX group, 53.25% ± 5.84%, n = 6 mice; ChR2 + PTX group, 58.82% ± 6.32%, n = 6 mice; $F_{2,18}$ = 17.99, p < 0.0001, one-way ANOVA with Tukey's post hoc test).

(I and J) Percentage of time spent in photoactivation-paired (I) (ChR2 group, 66.01% ± 4.72%; mCherry group, 44.13% ± 4.62%; n = 16 mice for each group; p = 0.002; $t_{(30)}$ = 3.31; two-tailed t test) or photoinhibition-paired chamber (J) (NpHR group, 30.11% ± 4.62%; mCherry group, 47.14% ± 5.26%; n = 13 and 14 mice for NpHR and mCherry groups, respectively; p = 0.02; $t_{(25)}$ = 2.42; two-tailed t test) when opsins were expressed in cVTA GABAergic neurons.

(K) Preference for the chamber paired with cVTA→DRN inhibitory circuit photoactivation was inhibited by microinjection of PTX into the DRN (ChR2 + vehicle group, 68.22% ± 5.87%, n = 7 mice; mCherry + PTX group, 48.07% ± 6.45%, n = 6 mice; ChR2 + PTX group, 47.41% ± 2.95%, n = 6 mice; $F_{2,16}$ = 5.02, p = 0.02, one-way ANOVA with Tukey's post hoc test).

*p < 0.05, **p < 0.01, ***p < 0.001; n.s., no significant difference. Error bars represent SEM.

See also Figures S5 and S6.

change in motor function or state of anxiety, as photoactivation of the R-C VTA→DRN inhibitory circuits had no influence on total distance traveled in the open field test or time spent in the open arm in the elevated plus maze (Figures S6A–S6E).

MOPs Are Expressed on rVTA GABAergic Terminals, but Not on cVTA GABAergic Terminals

Opioid receptors are expressed at high levels in brain areas related to reward (Le Merrer et al., 2009). MOPs on VTA GABAergic neurons are thought to be critically involved in opioid reward (Fields and Margolis, 2015). We sought to determine whether MOPs were also expressed in the reward-related inhibitory circuits between the R-C VTA and DRN.

To directly verify the locations of MOPs, we injected AAV5-ef1α-DIO-mGFP into the R-C VTA of Gad2-IRES-Cre mice and evaluated the coexistence of R-C VTA GABAergic terminals and MOPs in the DRN 2 weeks later. MOPs were highly co-localized with rVTA GABAergic terminals in the DRN (Figure 5A, top

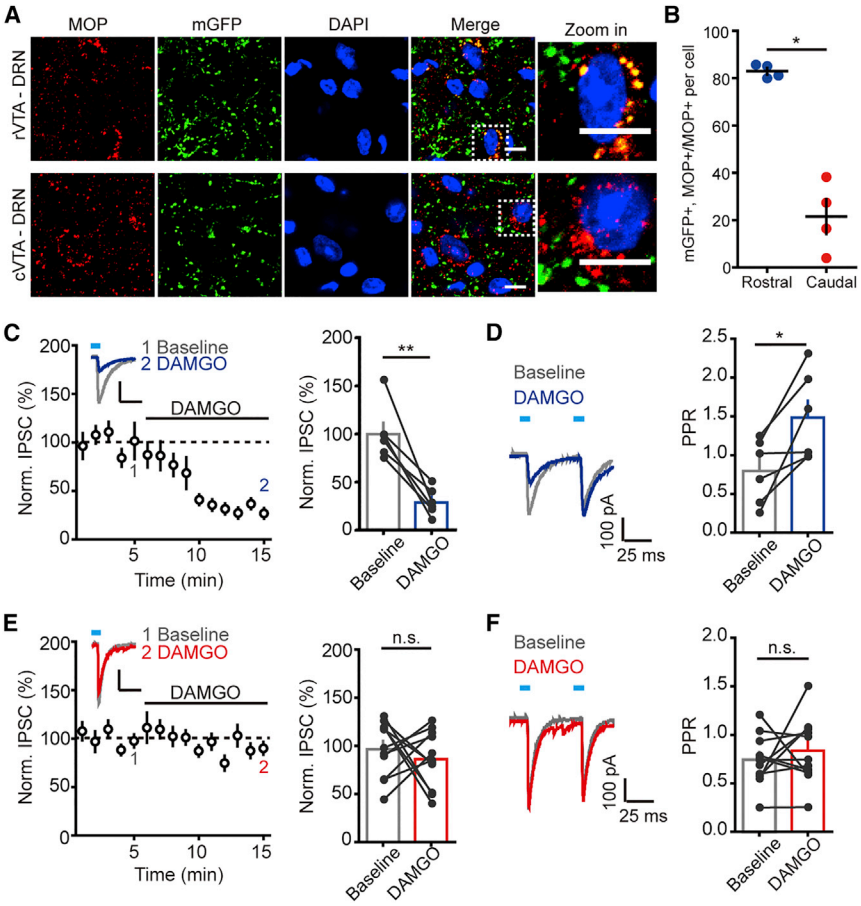

Figure 5. rVTA→DRN, but Not cVTA→DRN, GABAergic Terminals Expressed MOPs

(A) Expression of MOPs (red) at rostral (upper) and caudal (lower) VTA GABAergic terminals (green) in the DRN.

(B) Proportion of mGFP+ and MOP+ boutons in total MOP+ boutons per cell (among MOP positive boutons, 82.96% ± 1.42% and 21.53% ± 7.35% were also mGFP positive for rVTA and cVTA terminals; n = 4 mice for each group; p = 0.029; $U = 0$; Mann-Whitney test).

(C) rVTA→DRN eIPSCs were depressed by bath application of DAMGO (28.84% ± 5.81% of baseline; n = 6 neurons from 3 mice; p = 0.003; $t_{(5)} = 5.387$; paired t test).

(D) Example traces (left) and quantification (right) of PPR at rVTA→DRN synapses before (gray) and after (blue) DAMGO application (baseline, 0.79 ± 0.17; DAMGO, 1.48 ± 0.23; n = 6 neurons from 3 mice; p = 0.02; $t_{(5)} = 3.35$; paired t test).

(E) cVTA→DRN eIPSCs were not altered by bath application of DAMGO (86.12% ± 8.91% of baseline; n = 11 neurons from 3 mice; p = 0.52; $t_{(10)} = 0.67$; paired t test).

(F) Example traces (left) and quantification (right) of PPR at cVTA→DRN synapses before (gray) and after (red) DAMGO application (baseline, 0.74 ± 0.08; DAMGO, 0.84 ± 0.10; n = 11 neurons from 3 mice; p = 0.46; $t_{(10)} = 0.77$; paired t test).

*p < 0.05, **p < 0.001. n.s., no significant difference. Scale bars represent 10 μm(A) and 100 pA/25 ms (C and E). Error bars represent SEM. See also Figure S6.

panel, and Figure 5B), but few MOPs were co-localized with cVTA GABAergic terminals (Figure 5A, bottom panel, and Figure 5B). These results suggest that in the DRN, MOPs were mainly expressed on rVTA GABAergic terminals, but not on cVTA terminals, even on DRN local neurons. The resting membrane potentials of DRN GABAergic and non-GABAergic neurons were not affected by bath perfusion of [D-Ala2, NMe-Phe4, Gly-ol5]-enkephalin (DAMGO) (Figures S6F–S6H), indicating that DRN local neurons were not sensitive to MOP agonists, consistent with the above staining results.

To further investigate the different effects of MOPs on R-C VTA terminals, we expressed ChR2 in R-C VTA GABAergic neurons, perfused slices containing the DRN with the MOP agonist DAMGO (1 μM), and recorded eIPSCs. DAMGO incubation elicited a depression of eIPSCs in the rVTA→DRN circuit (Figure 5C), with an increase in the paired-pulse ratio (PPR) (Figure 5D), but not in the cVTA→DRN circuit eIPSCs or PPR (Figures 5E and 5F). Based on these findings, MOP activation decreased GABA release at rVTA→DRN synapses, but not at cVTA→DRN synapses, further indicating that MOPs existed on rVTA→DRN GABAergic terminals, but not on cVTA→DRN GABAergic terminals. DAMGO bath perfusion at a concentration of 1 μM may also activate δ-opioid receptors (DOPs) (Banghart et al., 2015). To investigate if DAMGO-mediated inhibition of the rVTA→DRN pathway was MOP specific, we perfused a cocktail of the DOP antagonist ICI 174,864 (3 μM) and DAMGO (1 μM) followed by a cocktail of the MOP-specific antagonist D-Phe-Cys-Tyr-D-Trp-Orn-Thr-Pen-Thr-NH2 (CTOP) (1 μM) and DAMGO (1 μM). ICI 174,864 did not affect the percentage of inhibition by DAMGO, but CTOP fully reversed the DAMGO-induced inhibition of the rVTA→DRN pathway (Figure S6I), indicating that MOP, but not DOP, existed at the rVTA→DRN GABAergic synapses.

As activation of the rVTA→DRN inhibitory pathway produced aversion (Figure 4C), we speculated that microinjecting MOP agonist DAMGO into the DRN might attenuate the aversive behavioral outcomes by depressing rVTA→DRN GABA transmission. To address this assumption, we microinjected DAMGO (1 mM) into the DRN 10 min before the RTPA experiment, in which mice received photoactivation of the rVTA→DRN inhibitory pathway. Place aversion was blocked by DAMGO pretreatment (Figure S6J), consistent with the electrophysiology results. In repeated morphine-treated mice, the RTPA was no longer inhibited by DAMGO (Figure S6K), reflecting the development of tolerance.

Based on these results, we proposed that within the DRN, MOPs were located on rVTA GABAergic terminals, but not cVTA GABAergic terminals. Activation of presynaptic MOPs inhibited rVTA GABAergic transmission in the DRN and blocked aversive outcomes induced by activating the rVTA→DRN

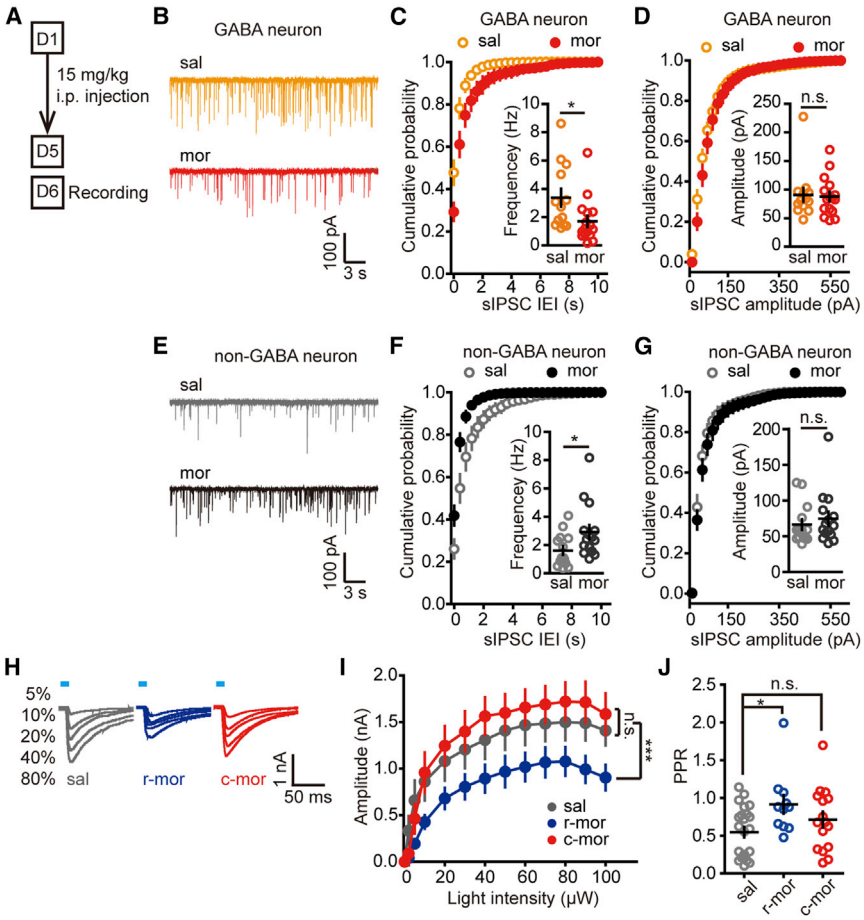

Figure 6. Opioids Depressed rVTA→DRN Inhibitory Neuronal Transmission without Affecting the cVTA→DRN Circuit

(A) Diagram of the morphine treatment procedure.

(B and E) Representative traces of sIPSCs in DRN GABAergic (B) and non-GABAergic (E) neurons.

(C and D) Cumulative probability distributions of the frequency (C) (saline, 3.37 ± 0.64 Hz; morphine, 1.71 ± 0.4 Hz; p = 0.02; D = 0.56; Kolmogorov-Smirnov test) and amplitude (D) (saline, 90.69 ± 12.18 pA; morphine, 87.89 ± 8.53 pA; p = 0.98; D = 0.17; Kolmogorov-Smirnov test) of sIPSCs in DRN GABAergic neurons (n = 13 and 16 neurons from 3 mice for the saline- and morphine-treated groups, respectively).

(F and G) Cumulative probability distributions of the frequency (F) (saline, 1.61 ± 0.31 Hz; morphine, 2.92 ± 0.49 Hz; p = 0.05; D = 0.50; Kolmogorov-Smirnov test) and amplitude (G) (saline, 66.16 ± 7.44 pA; morphine, 74.5 ± 9.61 pA; p = 0.77; D = 0.25; Kolmogorov-Smirnov test) of sIPSCs in DRN non-GABAergic neurons (n = 14 and 15 neurons from 3 mice for the saline- and morphine-treated groups, respectively).

(H) Representative traces of eIPSCs observed after stimulation with different light intensities.

(I) I/O curve of eIPSC amplitudes in response to different treatments (n = 23, 26, and 21 neurons from 4, 3, and 3 mice for saline, r-mor, and c-mor groups, respectively; $F_{2,793}$ = 31.21, p < 0.0001, two-way ANOVA).

(J) PPR values for different treatments (saline, 0.54 ± 0.07; r-mor, 0.92 ± 0.12; c-mor, 0.71 ± 0.10; n = 23, 11, and 16 neurons for saline, r-mor, and c-mor groups, respectively; $F_{2,47}$ = 3.67, p = 0.03, one-way ANOVA with Tukey's post hoc test).

*p < 0.05, ***p < 0.001; n.s., no significant difference. Error bars represent SEM. c-mor, morphine group expressing ChR2 in cVTA GABAergic neurons; r-mor, morphine group expressing ChR2 in rVTA GABAergic neurons; We pooled data from r-sal and c-sal in (H)–(J) because they were similar. See also Figure S7.

pathway, whereas DRN local neurons were not sensitive to MOP agonists.

Repeated Exposure to Morphine Depresses rVTA→DRN Inhibitory Transmission without Affecting cVTA→DRN Inhibitory Transmission

The different distributions of MOPs in R-C VTA terminals might lead to different effects of opioids on the two circuits. Morphine is a commonly used clinical opioid with high affinity toward MOPs and is strongly associated with addiction and abuse. We evaluated the influence of chronic morphine administration on the synaptic plasticity of the R-C VTA→DRN circuits. We intraperitoneally (i.p.) injected mice with morphine (15 mg/kg) for 5 days. The mice were sacrificed 12 hr after the last injection, brain slices that contained the VTA and DRN were prepared (Figure 6A), and synaptic transmission between the R-C VTA and DRN was evaluated.

First, we recorded sIPSCs in DRN GABAergic and non-GABAergic neurons after morphine exposure to evaluate inhibitory transmission in different DRN neurons. Compared with saline-treated mice, morphine-treated mice showed a decreased frequency of sIPSCs in DRN GABAergic neurons (Figures 6B and 6C), without changes in sIPSC amplitude (Figures 6B and 6D). In DRN non-GABAergic neurons, the sIPSC frequency was increased in the morphine group (Figures 6E and 6F), accompanied by an unaltered amplitude (Figures 6E and 6G). Thus, repeated treatment with morphine may decrease inhibitory transmission in DRN GABAergic neurons. This depression would disinhibit DRN local GABAergic neurons, thus resulting in increased inhibitory transmission in DRN serotonergic neurons.

To verify the influence of chronic morphine administration on neuronal transmission in the R-C VTA→DRN circuits, we recorded eIPSCs in the R-C VTA→DRN circuits of saline- and morphine-treated mice in response to stimulation with different intensities of light and generated input-output (I/O) curves. No differences in the I/O curves of the saline- and morphine-treated cVTA (c-mor) groups were observed (Figures 6H and 6I), but the I/O curve in the morphine-treated rVTA (r-mor) group shifted downward (Figure 6I), indicating depression of inhibitory transmission from the rVTA to DRN by chronic morphine administration. The PPR value increased at rVTA→DRN, but not cVTA→DRN, synapses (Figure 6J), thus indicating that depression of rVTA→DRN synaptic transmission occurred via a presynaptic mechanism.

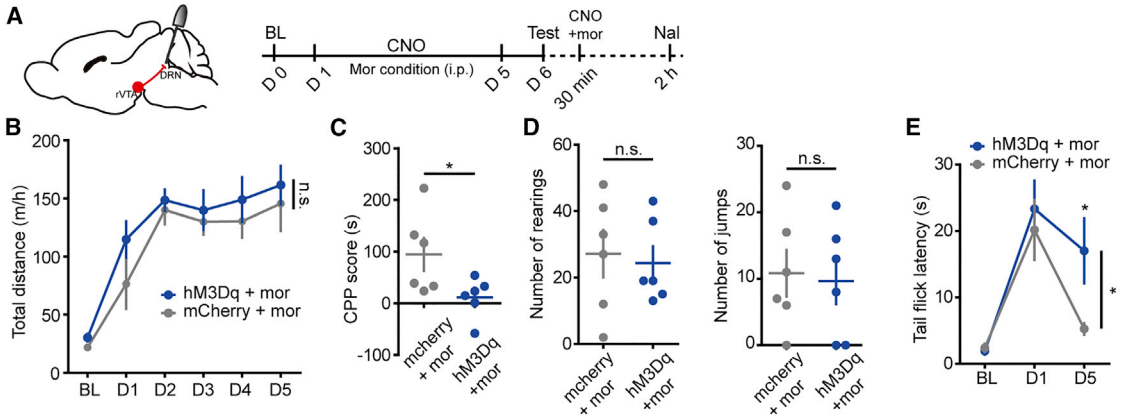

Figure 7. Role of the rVTA→DRN Circuit in Morphine-Adaptive Behaviors

(A) Drug administration and behavioral test procedures.

(B) Total distance traveled in response to morphine administration while chronically elevating rVTA→DRN circuit activity (n = 6 and 8 mice for mCherry and hM3Dq groups, respectively; $F_{1,68}$ = 3.4, p = 0.07, two-way ANOVA).

(C) CPP scores for mice following chronic activation of the rVTA→DRN circuit (CPP score = 94.63 ± 31.72 and 11.47 ± 15.66 s for mCherry and hM3Dq groups, respectively; n = 6 mice for each group; p = 0.04; $t_{(10)}$ = 2.35; two-tailed t test).

(D) Rearing (left) and jump number (right) after naloxone administration in mice following chronic activation of the rVTA→DRN circuit during morphine treatment (rearing number = 27.17 ± 7.12 and 24.33 ± 5.10 for mCherry and hM3Dq groups, respectively; n = 6 mice for each group; p = 0.75; $t_{(10)}$ = 0.32; two-tailed t test; jump number = 10.83 ± 3.50 and 9.67 ± 3.51 for mCherry and hM3Dq groups, respectively; n = 6 mice for each group; p = 0.82; $t_{(10)}$ = 0.24; two-tailed t test).

(E) Tail flick latency on different days for mice following chronic activation of the rVTA→DRN circuit (n = 6 mice for each group; $F_{1,10}$ = 6.24, p = 0.03, repeated two-way ANOVA) during morphine treatment.

*p < 0.05, n.s., no significant difference. Error bars represent SEM.

See also Figure S8.

These data suggest that repeated morphine treatment depressed rVTA→DRN GABAergic transmission presynaptically, whereas cVTA→DRN GABAergic transmission remained unaltered.

To further support that transmission in the rVTA→DRN pathway was depressed presynaptically by repeated morphine exposure, we expressed ChR2 in rVTA GABAergic neurons and recorded light-evoked quantal events (qIPSC) in DRN GABAergic neurons by replacing extracellular calcium (Ca^{2+}) with strontium (Sr^{2+}) to desynchronize release (Oliet et al., 1996) (Figure S7A). The frequencies, but not amplitudes, of qIPSCs were decreased in the morphine-treated mice compared with saline-treated mice (Figures S7B–S7D), indicating a decrease in release sites at rVTA→DRN synapses instead of a postsynaptic mechanism.

Repeated morphine administration may influence the endogenous opioid system. We compared the impact of DAMGO on rVTA→DRN eIPSCs in morphine-treated and untreated mice. The percentage of inhibition by DAMGO was lower in morphine-treated mice (Figures S7E and S7F), reflecting the development of tolerance. The impact of opioid receptor antagonist naloxone on rVTA→DRN eIPSCs in morphine-treated and untreated mice was also measured. The percentage of potentiation by naloxone was significantly higher in morphine-treated mice (Figures S7G and S7H), signifying an increased endogenous opioid tone within this pathway after chronic morphine treatment, which may explain why repeated morphine exposure depressed this pathway. The mechanism of tolerance might be either the desensitization of MOPs or occlusion by increased endogenous opioids, which need further investigation.

The Rostral VTA→DRN Pathway Is Critical in Morphine Reward

To test if the rVTA→DRN pathway is involved in the development of morphine dependence, we measured morphine-induced locomotor, conditioned place preference (CPP), withdrawal, and tolerance-related behaviors while modulating neuronal activity of this circuit (see Method Details). We expressed chemogenetic receptor hM3Dq in rVTA GABAergic neurons and microinjected clozapine-N-oxide (CNO) into the DRN 5 min before morphine application to chronically activate rVTA→DRN GABAergic terminals during morphine administration (Figures 7A and S8). The total distance traveled 1 hr after morphine administration and the CPP score were measured, and withdrawal behaviors were induced by injecting opioid receptor antagonist naloxone after 5 days of morphine conditioning (Figure 7A). Analgesic effects and tolerance of morphine were measured by tail flick latency (see Method Details).

Chemogenetic activation of the rVTA→DRN GABAergic terminals had no effect on morphine-induced hyperactivity (Figure 7B). However, the CPP scores significantly decreased (Figure 7C), indicating that activation of the rVTA→DRN pathway might disrupt the rewarding effects of morphine. Rearing and jumping reflect somatic signs of withdrawal; however, the number of rears and jumps was not affected by activating the pathway during drug administration (Figure 7D). In the tail flick test, latency was largely increased by morphine administration on day 1 in both groups (Figure 7E), suggesting that the pain-relieving effects of morphine were not affected by activation of rVTA→DRN terminals. After 4 days of repeated morphine administration at the same dosage, the latency of the control

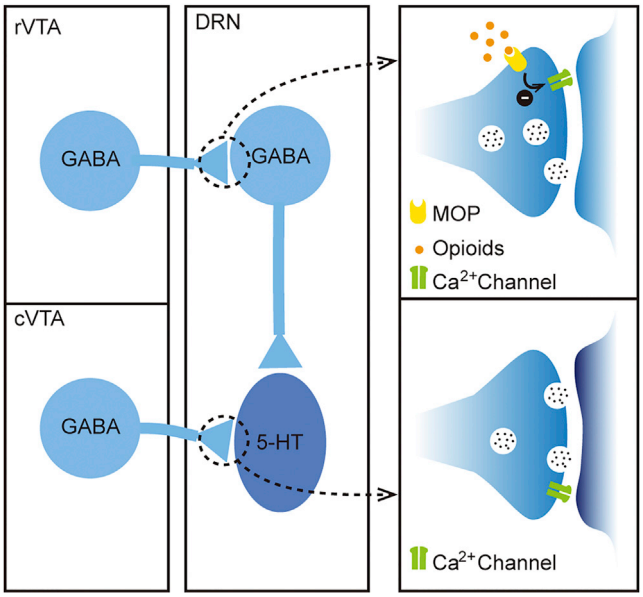

Figure 8. Hypothetical Model of the Microcircuit between the VTA and DRN

Rostral VTA GABAergic neurons preferentially target DRN GABAergic neurons and disinhibit DRN serotonergic neurons; caudal VTA GABAergic neurons directly inhibit DRN serotonergic neurons. MOPs are expressed on the terminals of the rVTA→DRN circuit, but not on the terminals of the cVTA→DRN circuit. GABA release from rVTA→DRN synapses is inhibited by repeated administration of morphine.

group decreased to the baseline level, reflecting the development of tolerance. However, the latency was higher in the hM3Dq group, demonstrating that activation of the rVTA→DRN pathway during drug administration may prevent the development of tolerance to some extent (Figure 7E). These data suggest that the rVTA→DRN pathway specifically contributes to morphine reward without affecting the analgesic effects of morphine.

DISCUSSION

We investigated the precise connections between the VTA and DRN and the functions of these circuits using rabies virus tracing, electrophysiology, and behavioral assays. We showed that projections from the VTA to DRN were GABAergic, and R-C VTA GABAergic neurons targeted different DRN neurons. Beyond the differences in downstream cell types, the plasticity of the R-C VTA→DRN circuits was differentially modulated by opioids. The rVTA→DRN pathway specifically modulated morphine-induced CPP (Figure 8).

The rVTA is continuous with the lateral hypothalamus and supramammillary nucleus, and the cVTA is located dorsolateral to the interpeduncular nucleus (Sanchez-Catalan et al., 2014). These two areas are located relatively close to each other. Thus, we carefully checked the expression patterns of viruses within the R-C VTA (Figure S5). Indeed, some virus expression was found beyond the R-C VTA boundary, but the center of virus expression was located at the R-C VTA. A major problem is that the cVTA is close to the tail VTA (tVTA; also known as RMtg), which is enriched in GABAergic neurons. As shown in Figures S5C and S5E, the virus expressions were concentrated in the cVTA, but not the tVTA. However, we could not avoid some infection in the rostral part of the tVTA due to its overlap with the caudal cVTA (Sanchez-Catalan et al., 2014). It has been reported that the tVTA terminals are concentrated in the central part of the DRN (Sego et al., 2014), similar to our results in Figure S5D. This indicates that the cVTA and tVTA might innervate similar populations of DRN neurons. tVTA GABAergic neurons can be activated by psychostimulant drugs and highly expressed MOPs (Jhou et al., 2009; Quina et al., 2015; Schifirneț et al., 2014). Although we found that cVTA-DRN GABAergic terminals rarely expressed MOPs, it would be interesting to investigate whether tVTA→DRN synapses are modulated by opioids and compare them with the cVTA→DRN pathway. Further neuroanatomical, pharmacological, and electrophysiological studies are needed to determine whether the cVTA in our study is the same as the tVTA.

In our study, different VTA GABAergic neurons inhibited or disinhibited DRN serotonergic neurons through direct inhibition or DRN GABAergic neuron-mediated disinhibition. This very much resembles the excitatory inputs to the DRN from the LHb (Zhou et al., 2017) and mPFC (Geddes et al., 2016); both DRN serotonergic and GABAergic neurons receive excitatory inputs, resulting in direct excitation and GABAergic neuron-mediated feed-forward inhibition of serotonergic neurons. Retina ganglion cells inhibit DRN serotonergic neurons through activating DRN GABAergic neurons (Huang et al., 2017). In our research, the excitatory or inhibitory inputs to the DRN are modulated elaborately through DRN local microcircuits. DRN local GABAergic to serotonergic neuronal synapses are apparently important for regulating the homeostasis of specific pathways and modulating the excitation and inhibition balance of DRN serotonergic neurons.

Interestingly, we found that activation of R-C VTA→DRN inhibitory inputs resulted in opposite outcomes in reward-related behaviors. These two groups of neurons oppositely modulated serotonergic neuronal activity and function. This conclusion is consistent with the theory that serotonergic neurons signal punishment and inhibit behavior (Cohen et al., 2015; Crockett et al., 2009; Dayan and Huys, 2009). However, recent findings indicate that activation of DRN serotonergic neurons is reinforcing (Li et al., 2016; Liu et al., 2014). These different behavioral outcomes between our results and other studies might be due to the different methods used and/or different subtype of neurons manipulated. Fiber photometry recordings reflect the acute responses to reward of all serotonergic neurons (Li et al., 2016). Optogenetic activation of DRN serotonergic neurons acutely excites the whole serotonergic neuronal population (Liu et al., 2014). However, serotonergic neurons within the DRN are relatively heterogeneous and are reported to respond to both reward and punishment on different timescales (Cohen et al., 2015; Ren et al., 2018). In the current study, we used optogenetics to manipulate GABAergic inputs to the DRN to inhibit or elevate the basal activity of local DRN circuits *in vivo*. The R-C VTA GABAergic neurons may directly or indirectly influence a subset of DRN serotonergic neurons, whose tonic activation reflects

negative values of emotion. How different subpopulations of serotonergic neurons respond to reward and aversion on different timescales remains to be studied. In addition, previous research shows that microinjecting $GABA_AR$ antagonists into the rVTA is rewarding (Ikemoto et al., 1997) and microinjecting agonists into the cVTA is aversive (Ikemoto et al., 1998), whereas our results suggest that activation of rVTA→DRN GABAergic inputs produces aversion. These different behavioral outcomes could result from the manipulation of different pathways and neurons; pharmacological manipulation disinhibits all neurons, especially dopaminergic neurons, within the rVTA. We focused on the rVTA→DRN inhibitory pathway and assumed that a subset of serotonergic neurons within the DRN contributed to the aversive outcomes.

Endogenous opioids and their receptors are widely distributed in the CNS, including in the VTA and periaqueductal gray (PAG) (Le Merrer et al., 2009; Trigo et al., 2010). MOPs are primarily distributed in VTA interneurons and GABAergic afferents to the VTA (Hjelmstad et al., 2013; Jalabert et al., 2011; Matsui et al., 2014). However, the mechanism by which the endogenous opioid system influences VTA GABAergic projection neurons is not clear. It is reported that GABAergic neurons in the VTA are relatively insensitive to morphine-induced presynaptic inhibition, and the inhibition of eIPSCs recorded on VTA dopaminergic neurons by light activation of VTA interneurons is relatively small (~11%) (Matsui et al., 2014). However, we found rVTA→DRN GABAergic terminals to be much more sensitive to morphine (percentage of inhibition of 71.16% ± 5.81%). This indicates that VTA GABAergic interneurons and projection neurons are differently modulated by morphine. Another possibility is that the expression and distribution levels of MOPs differed on the somas and terminals of local interneurons and projection neurons. The VTA interneurons may be more sensitive to opioids at soma-dendrite sites, whereas projection neurons may be more sensitive to opioids at terminals. Unexpectedly, we found a large proportion of MOPs within the DRN were located on GABAergic terminals originating from the rVTA, but not on local neurons within the DRN. These results are consistent with previous study showing that MOP mRNA expression can only be seen in the caudal portion of the DRN at a very low level (Mansour et al., 1994). The influence of opioids on DRN neurons might be through afferents to the DRN such as the rVTA or through other opioid receptor subtypes such as κ-opioid receptors, which are highly expressed in the DRN.

Addictive drugs are thought to induce long-lasting synaptic remodeling (Lüscher and Malenka, 2011). VTA GABAergic neurons are critical targets of opioids (Fields and Margolis, 2015). In the current study, reward-related VTA→DRN inhibitory circuits were also found to be modulated by opioids. Repeated morphine treatment depressed rVTA→DRN GABAergic synapse transmission in DRN GABAergic neurons. This depression removed the inhibition of local DRN GABAergic neurons, thus resulting in subsequent inhibition of DRN serotonergic neurons. Decreased activities of DRN serotonergic neurons are directly associated with increased levels of impulsivity (Grigor'ian, 2011; Harrison et al., 1997; Kirby et al., 2011). In our study, chronic morphine administration may have induced impulsive drug-seeking behavior partly through the inhibition of serotonergic neurons. This was also established by our chronic activation of the rVTA→DRN pathway in the morphine administration period. Conditioned preference for morphine was disrupted, indicating that this pathway may be necessary for the expression of morphine-induced drug seeking. Chemogenetic activation of the rVTA→DRN inhibitory circuit blocked morphine-induced CPP without affecting other behaviors. This indicates that the rVTA→DRN inhibitory pathway specifically modulated morphine reward. Other adaptive behaviors might be associated with other opioid receptors or circuits. Our results identified the rVTA→DRN inhibitory circuit as another key system mediating morphine reward. Activating this pathway during opioid administration may be a new strategy to reduce the addiction properties without affecting the analgesic effects.

Taken together, our results suggest that rVTA GABAergic neurons disinhibited a subpopulation of DRN serotonergic neurons whose tonic activation reflected negative values of emotion; the rVTA→DRN pathway specifically gated morphine reward by indirectly modulating this subset of serotonergic neurons via presynaptic MOPs. Our research provides insight into VTA-DRN interaction patterns and reveals new targets for studies on opioid dependence.

STAR★METHODS

Detailed methods are provided in the online version of this paper and include the following:

- KEY RESOURCES TABLE
- CONTACT FOR REAGENT AND RESOURCE SHARING
- EXPERIMENTAL MODEL AND SUBJECT DETAILS
- METHOD DETAILS
  - Virus
  - Stereotaxic injections
  - Histology and imaging
  - Acute brain slice preparation
  - *In vitro* electrophysiology
  - *In vivo* local field potential recordings
  - Real-time place preference/aversion
  - Open field test
  - Elevated plus maze test
  - Morphine-induced locomotor, CPP, and withdrawal
  - Tail flick test
  - Cannula implantation and *in vivo* opto-stimulation
- QUANTIFICATION AND STATISTICAL ANALYSIS

SUPPLEMENTAL INFORMATION

Supplemental Information includes eight figures and can be found with this article online at https://doi.org/10.1016/j.neuron.2018.12.012.

ACKNOWLEDGMENTS

We thank T.F. Yuan (Shanghai Jiao Tong University, China), M.M. Luo (National Institute of Biological Sciences, China), L. Lu (Peking University, China), H.L. Hu, J.D. Chen (Zhejiang University, China), and members of the X.M. Li laboratory for comments on the experimental design and manuscript. We thank L.P. Wang (Shenzhen Institute of Advanced Technology, Chinese Academy of Sciences, China) for providing the virus expressing opsins, J. Hu (Shanghai Technology University, China) for providing the AAV5-ef1α-DIO-mGFP virus,

and Y. Rao and M.M. Luo for kindly providing the mouse lines. This work was supported by the Key Project of the National Natural Science Foundation of China (31430034), the Major Research Plan of the National Natural Science Foundation of China (91432306), the National Key Research and Development Plan of Ministry of Science and Technology of China (2016YF051000), the Non-Profit Central Research Institute Fund of the Chinese Academy of Medical Sciences (2018PT31041), and Funds for Creative Research Groups of China from the National Natural Science Foundation of China (81521062).

AUTHOR CONTRIBUTIONS

Conceptualization, Y.L. and X.-M.L; Methodology, Y.L. and C.-Y.L; Formal Analysis, Y.L., C.-Y.L., W.X., S.J., and Z.-H.W.; Investigation, Y.L., C.-Y.L., X.W., S.J., Z.-H.W., and P.J.; Writing – Original Draft, Y.L.; Writing – Review & Editing, Y.L., C.-Y.L. P.D., X.-B.H, F.-Q.X., S.D., Y.-D.Z., and X.-M.L.; Supervision, X.-M.L.; Funding Acquisition, X.-M.L.

DECLARATION OF INTERESTS

The authors declare no competing financial interests.

Received: June 25, 2018
Revised: October 26, 2018
Accepted: December 7, 2018
Published: January 10, 2019

REFERENCES

Banghart, M.R., Neufeld, S.Q., Wong, N.C., and Sabatini, B.L. (2015). Enkephalin disinhibits Mu opioid receptor-rich striatal patches via delta opioid receptors. Neuron *88*, 1227–1239.

Bromberg-Martin, E.S., Matsumoto, M., and Hikosaka, O. (2010). Dopamine in motivational control: rewarding, aversive, and alerting. Neuron *68*, 815–834.

Cohen, J.Y., Amoroso, M.W., and Uchida, N. (2015). Serotonergic neurons signal reward and punishment on multiple timescales. eLife *4*, e06346.

Crockett, M.J., Clark, L., and Robbins, T.W. (2009). Reconciling the role of serotonin in behavioral inhibition and aversion: acute tryptophan depletion abolishes punishment-induced inhibition in humans. J. Neurosci. *29*, 11993–11999.

Dayan, P., and Huys, Q.J. (2009). Serotonin in affective control. Annu. Rev. Neurosci. *32*, 95–126.

Fields, H.L., and Margolis, E.B. (2015). Understanding opioid reward. Trends Neurosci. *38*, 217–225.

Geddes, S.D., Assadzada, S., Lemelin, D., Sokolovski, A., Bergeron, R., Haj-Dahmane, S., and Béïque, J.C. (2016). Target-specific modulation of the descending prefrontal cortex inputs to the dorsal raphe nucleus by cannabinoids. Proc. Natl. Acad. Sci. USA *113*, 5429–5434.

Grigor'ian, G.A. (2011). [Serotonin and impulsivity (experiments on animals)]. Zh. Vyssh. Nerv. Deiat. Im. I P Pavlova *61*, 261–273.

Harrison, A.A., Everitt, B.J., and Robbins, T.W. (1997). Central 5-HT depletion enhances impulsive responding without affecting the accuracy of attentional performance: interactions with dopaminergic mechanisms. Psychopharmacology (Berl.) *133*, 329–342.

Hjelmstad, G.O., Xia, Y., Margolis, E.B., and Fields, H.L. (2013). Opioid modulation of ventral pallidal afferents to ventral tegmental area neurons. J. Neurosci. *33*, 6454–6459.

Huang, L., Yuan, T., Tan, M., Xi, Y., Hu, Y., Tao, Q., Zhao, Z., Zheng, J., Han, Y., Xu, F., et al. (2017). A retinoraphe projection regulates serotonergic activity and looming-evoked defensive behaviour. Nat. Commun. *8*, 14908.

Ikemoto, S., Murphy, J.M., and McBride, W.J. (1997). Self-infusion of GABA(A) antagonists directly into the ventral tegmental area and adjacent regions. Behav. Neurosci. *111*, 369–380.

Ikemoto, S., Murphy, J.M., and McBride, W.J. (1998). Regional differences within the rat ventral tegmental area for muscimol self-infusions. Pharmacol. Biochem. Behav. *61*, 87–92.

Jacobs, B.L., and Azmitia, E.C. (1992). Structure and function of the brain serotonin system. Physiol. Rev. *72*, 165–229.

Jalabert, M., Bourdy, R., Courtin, J., Veinante, P., Manzoni, O.J., Barrot, M., and Georges, F. (2011). Neuronal circuits underlying acute morphine action on dopamine neurons. Proc. Natl. Acad. Sci. USA *108*, 16446–16450.

Jhou, T.C., Geisler, S., Marinelli, M., Degarmo, B.A., and Zahm, D.S. (2009). The mesopontine rostromedial tegmental nucleus: A structure targeted by the lateral habenula that projects to the ventral tegmental area of Tsai and substantia nigra compacta. J. Comp. Neurol. *513*, 566–596.

Johnson, S.W., and North, R.A. (1992). Opioids excite dopamine neurons by hyperpolarization of local interneurons. J. Neurosci. *12*, 483–488.

Jolas, T., Nestler, E.J., and Aghajanian, G.K. (2000). Chronic morphine increases GABA tone on serotonergic neurons of the dorsal raphe nucleus: association with an up-regulation of the cyclic AMP pathway. Neuroscience *95*, 433–443.

Kirby, L.G., Zeeb, F.D., and Winstanley, C.A. (2011). Contributions of serotonin in addiction vulnerability. Neuropharmacology *61*, 421–432.

Le Merrer, J., Becker, J.A., Befort, K., and Kieffer, B.L. (2009). Reward processing by the opioid system in the brain. Physiol. Rev. *89*, 1379–1412.

Li, Y., Zhong, W., Wang, D., Feng, Q., Liu, Z., Zhou, J., Jia, C., Hu, F., Zeng, J., Guo, Q., et al. (2016). Serotonin neurons in the dorsal raphe nucleus encode reward signals. Nat. Commun. *7*, 10503.

Liu, Z., Zhou, J., Li, Y., Hu, F., Lu, Y., Ma, M., Feng, Q., Zhang, J.E., Wang, D., Zeng, J., et al. (2014). Dorsal raphe neurons signal reward through 5-HT and glutamate. Neuron *81*, 1360–1374.

Lüscher, C., and Malenka, R.C. (2011). Drug-evoked synaptic plasticity in addiction: from molecular changes to circuit remodeling. Neuron *69*, 650–663.

Mansour, A., Fox, C.A., Burke, S., Meng, F., Thompson, R.C., Akil, H., and Watson, S.J. (1994). Mu, delta, and kappa opioid receptor mRNA expression in the rat CNS: an in situ hybridization study. J. Comp. Neurol. *350*, 412–438.

Matsui, A., Jarvie, B.C., Robinson, B.G., Hentges, S.T., and Williams, J.T. (2014). Separate GABA afferents to dopamine neurons mediate acute action of opioids, development of tolerance, and expression of withdrawal. Neuron *82*, 1346–1356.

Ogawa, S.K., Cohen, J.Y., Hwang, D., Uchida, N., and Watabe-Uchida, M. (2014). Organization of monosynaptic inputs to the serotonin and dopamine neuromodulatory systems. Cell Rep. *8*, 1105–1118.

Oliet, S.H., Malenka, R.C., and Nicoll, R.A. (1996). Bidirectional control of quantal size by synaptic activity in the hippocampus. Science *271*, 1294–1297.

Pan, G., Li, Y., Geng, H.Y., Yang, J.M., Li, K.X., and Li, X.M. (2015). Preserving GABAergic interneurons in acute brain slices of mice using the N-methyl-D-glucamine-based artificial cerebrospinal fluid method. Neurosci. Bull. *31*, 265–270.

Paxinos, G., and Franklin, K.B.J. (2013). Paxinos and Franklin's the Mouse Brain in Stereotaxic Coordinates, Fourth Edition (Elsevier/Academic Press).

Pollak Dorocic, I., Fürth, D., Xuan, Y., Johansson, Y., Pozzi, L., Silberberg, G., Carlén, M., and Meletis, K. (2014). A whole-brain atlas of inputs to serotonergic neurons of the dorsal and median raphe nuclei. Neuron *83*, 663–678.

Polter, A.M., Barcomb, K., Tsuda, A.C., and Kauer, J.A. (2018). Synaptic function and plasticity in identified inhibitory inputs onto VTA dopamine neurons. Eur. J. Neurosci. *47*, 1208–1218.

Quina, L.A., Tempest, L., Ng, L., Harris, J.A., Ferguson, S., Jhou, T.C., and Turner, E.E. (2015). Efferent pathways of the mouse lateral habenula. J. Comp. Neurol. *523*, 32–60.

Ren, J., Friedmann, D., Xiong, J., Liu, C.D., Ferguson, B.R., Weerakkody, T., DeLoach, K.E., Ran, C., Pun, A., Sun, Y., et al. (2018). Anatomically defined and functionally distinct dorsal raphe serotonin sub-systems. Cell *175*, 472–487.e420.

Root, D.H., Mejias-Aponte, C.A., Zhang, S., Wang, H.L., Hoffman, A.F., Lupica, C.R., and Morales, M. (2014). Single rodent mesohabenular axons release glutamate and GABA. Nat. Neurosci. *17*, 1543–1551.

Sanchez-Catalan, M.J., Kaufling, J., Georges, F., Veinante, P., and Barrot, M. (2014). The antero-posterior heterogeneity of the ventral tegmental area. Neuroscience *282*, 198–216.

Schifirneț, E., Bowen, S.E., and Borszcz, G.S. (2014). Separating analgesia from reward within the ventral tegmental area. Neuroscience *263*, 72–87.

Sego, C., Gonçalves, L., Lima, L., Furigo, I.C., Donato, J., Jr., and Metzger, M. (2014). Lateral habenula and the rostromedial tegmental nucleus innervate neurochemically distinct subdivisions of the dorsal raphe nucleus in the rat. J. Comp. Neurol. *522*, 1454–1484.

Stamatakis, A.M., Jennings, J.H., Ung, R.L., Blair, G.A., Weinberg, R.J., Neve, R.L., Boyce, F., Mattis, J., Ramakrishnan, C., Deisseroth, K., and Stuber, G.D. (2013). A unique population of ventral tegmental area neurons inhibits the lateral habenula to promote reward. Neuron *80*, 1039–1053.

Tan, K.R., Brown, M., Labouèbe, G., Yvon, C., Creton, C., Fritschy, J.M., Rudolph, U., and Lüscher, C. (2010). Neural bases for addictive properties of benzodiazepines. Nature *463*, 769–774.

Tan, K.R., Yvon, C., Turiault, M., Mirzabekov, J.J., Doehner, J., Labouèbe, G., Deisseroth, K., Tye, K.M., and Lüscher, C. (2012). GABA neurons of the VTA drive conditioned place aversion. Neuron *73*, 1173–1183.

Trigo, J.M., Martin-García, E., Berrendero, F., Robledo, P., and Maldonado, R. (2010). The endogenous opioid system: a common substrate in drug addiction. Drug Alcohol Depend. *108*, 183–194.

van Zessen, R., Phillips, J.L., Budygin, E.A., and Stuber, G.D. (2012). Activation of VTA GABA neurons disrupts reward consumption. Neuron *73*, 1184–1194.

Vandermaelen, C.P., and Aghajanian, G.K. (1983). Electrophysiological and pharmacological characterization of serotonergic dorsal raphe neurons recorded extracellularly and intracellularly in rat brain slices. Brain Res. *289*, 109–119.

Watabe-Uchida, M., Zhu, L., Ogawa, S.K., Vamanrao, A., and Uchida, N. (2012). Whole-brain mapping of direct inputs to midbrain dopamine neurons. Neuron *74*, 858–873.

Weissbourd, B., Ren, J., DeLoach, K.E., Guenthner, C.J., Miyamichi, K., and Luo, L. (2014). Presynaptic partners of dorsal raphe serotonergic and GABAergic neurons. Neuron *83*, 645–662.

Wickersham, I.R., Lyon, D.C., Barnard, R.J., Mori, T., Finke, S., Conzelmann, K.K., Young, J.A., and Callaway, E.M. (2007). Monosynaptic restriction of transsynaptic tracing from single, genetically targeted neurons. Neuron *53*, 639–647.

Zhou, L., Liu, M.Z., Li, Q., Deng, J., Mu, D., and Sun, Y.G. (2017). Organization of functional long-range circuits controlling the activity of serotonergic neurons in the dorsal raphe nucleus. Cell Rep. *20*, 1991–1993.

STAR★METHODS

KEY RESOURCES TABLE

REAGENT or RESOURCE	SOURCE	IDENTIFIER
Antibodies		
Rabbit anti-GABAAR α1 subunit	Millipore	Cat# 06-868 RRID:AB_310272
Mouse anti-TH	Immunostar	Cat# 22941 RRID:AB_572268
Guinea pig anti-MOP	Millipore	Cat# AB5509 RRID:AB_177511
Rabbit anti-Tph2	Novus Biologicals	Cat# NB100-74555 RRID:AB_1049988
Goat anti-rabbit 549	Jackson ImmunoResearch	Cat# 111-505-003 RRID:AB_2493180
Donkey anti-rabbit 647	Invitrogen	Cat# A-31571 RRID:AB_162542
Goat anti-mouse 488	Jackson Immunoresearch	Cat# 115-545-003 RRID:AB_2338840
Goat anti-guinea pig 549	Jackson Immunoresearch	Cat# 106-165-003 RRID:AB_2337423
Bacterial and Virus Strains		
AAV5-ef1α-DIO-ChR2-mCherry	Laboratory of Li-Ping Wang	N/A
AAV5-ef1α-DIO-NpHR-mCherry	Laboratory of Li-Ping Wang	N/A
AAV5-Syn-ChR2-mCherry	Laboratory of Li-Ping Wang	N/A
AAV5-ef1α-DIO-mGFP	Laboratory of Ji Hu	N/A
AAV2/9-ef1a-DIO-hM3Dq-mCherry	BrainVTA, Wuhan, China	N/A
AAV9-CAG-DIO-RVG	Laboratory of Fu-Qiang Xu	N/A
AAV9-CAG-DIO-GFP-TVA	Laboratory of Fu-Qiang Xu	N/A
RV-EvnA-DsRed	Laboratory of Fu-Qiang Xu	N/A
Chemicals, Peptides, and Recombinant Proteins		
Biocytin	Sigma-Aldrich	Cat# B4261
Alexa Fluor 633-conjugated streptavidin	Invitrogen	Cat# S21375 RRID:AB_2313500
TTX	Tocris	Cat# 1078
4-AP	Sigma-Aldrich	Cat# 275875
PTX	Tocris	Cat# 3056
DNQX	Tocris	Cat# 0189
AP-V	Tocris	Cat# 0105
NE	Sigma-Aldrich	Cat# A7256-1G
Naloxone	Tocris	Cat# 0599
CNO	Sigma-Aldrich	Cat# 810611
DAMGO	Tocris	Cat# 1171
CTOP	Tocris	Cat# 1578
Strychnine	Toronto Research Chemicals	Cat# S687710
Bicuculline	Tocris	Cat# 0130
ICI 174,864	Tocris	Cat# 0820
CPA	Tocris	Cat# 1702
DPCPX	Tocris	Cat# 0439
Morphine-HCl	Shenyang Pharmaceutical	CFDA Approval# H21022436
Deposited Data		
8.267735	Figure S7H	Grubbs' test
Experimental Models: Organisms/Strains		
Mouse: Gad2-IRES-Cre (B6N.Cg-Gad2tm2(cre)Zjh/J)	The Jackson Laboratory	JAX: 019022 RRID: IMSR_JAX:019022
Mouse: ePet1-Cre (B6.Cg-Tg(Fev-cre)1Esd/J)	The Jackson Laboratory	JAX: 012712 RRID: IMSR_JAX:012712
Mouse: Ai9 (B6.Cg-Gt(ROSA)26Sortm9(CAG-tdTomato)Hze/J)	The Jackson Laboratory	JAX: 007909 RRID: IMSR_JAX:007909

(*Continued on next page*)

Continued

REAGENT or RESOURCE	SOURCE	IDENTIFIER
Software and Algorithms		
GraphPad Prism 5	GraphPad	https://www.graphpad.com/;RRID:SCR_002798
ImageJ	NIH	https://imagej.nih.gov/ij/; RRID:SCR_003070
pClamp 10.4	Molecular Devices	http://mdc.custhelp.com/; RRID:SCR_011323
Origin 8	OriginLab Corporation	https://store.originlab.com/; RRID:SCR_014212

CONTACT FOR REAGENT AND RESOURCE SHARING

Further information and requests for resources and reagents should be directed to and will be fulfilled by the Lead Contact, Xiao-Ming Li (lixm@zju.edu.cn).

EXPERIMENTAL MODEL AND SUBJECT DETAILS

Experiments were performed on adult Gad2-IRES-Cre (JAX Strain: 019022), ePet1-Cre (JAX Strain: 012712), and Ai9 (JAX Strain: 007909) mice. Four-week-old mice were used for virus injection experiments and 8–10-week-old mice were used for electrophysiology and behavioral experiments. For slice electrophysiology experiments, Gad2-IRES-Cre/ePet1-Cre mice were crossed with Ai9 mice to label GAD65-positive/serotonergic neurons with tdTomato. Male mice were used in behavioral tests, and both male and female mice were used in electrophysiology and immunohistochemistry experiments. Mice were singly housed after implantation of the guide cannula. All mice were housed at a constant temperature and humidity with a 12-h light/dark cycle. Experiments were done during the light phase. All procedures were approved by the Animal Advisory Committee at Zhejiang University and performed in accordance with the National Institutes of Health *Guidelines for the Care and Use of Laboratory Animals*.

METHOD DETAILS

Virus

For rabies virus-mediated transneuronal tracing, AAV9-CAG-DIO-RVG (titer, 6.5×10^{12} genome copies (gc)/ml), AAV9-CAG-DIO-GFP-TVA (titer, 5.3×10^{12} gc/ml), and EnvA-pseudotyped, glycoprotein (RG)-deleted rabies virus RV-EvnA-DsRed (titer, 2×10^{8} colony forming units (cfu)/ml) were provided by Fu-Qiang Xu's lab at the Wuhan Institute of Physics and Mathematics (WIPM). AAVs expressing opsins (AAV5-ef1α-DIO-ChR2-mCherry, titer, 5.56×10^{12} gc/ml; AAV5-ef1α-DIO-NpHR-mCherry, titer, 4.80×10^{12} gc/ml; AAV5-Syn-ChR2-mCherry, titer, 5.20×10^{12} gc/ml) were gifts from Li-Ping Wang's lab at the Shenzhen Institute of Advanced Technology (SIAT). AAV5-ef1α-DIO-mGFP (titer, 5.36×10^{12} gc/ml) was constructed by Ji Hu's lab at Shanghai Technology University. AAV2/9-ef1a-DIO-hM3Dq-mCherry (titer, 6.91×10^{12} gc/ml) was purchased from BrainVTA, Wuhan, China.

Stereotaxic injections

Mice were deeply anesthetized and placed in a stereotaxic apparatus (RWD, 68030, 68025, Shenzhen, China). During surgery and virus injection, anesthesia was maintained with isoflurane (1%). The skull above the targeted areas was thinned with a dental drill (STRONG, 90+102, Guangdong, China) and carefully removed. Injections were performed with a 10 μL syringe (Hamilton, Nevada, USA) connected to a glass micropipette with a 10–15 μm diameter tip. Syringe pumps (KD Scientific, 78-8130, USA) were used to inject the virus at a certain speed and volume.

To infect the VTA neurons with AAVs, we injected AAV5-ef1a-DIO-ChR2-mCherry, AAV5-ef1a-DIO-NpHR-mCherry, AAV5-ef1α-DIO-mGFP, or AAV2/9-ef1a-DIO-hM3Dq-mCherry bilaterally into the VTA of Gad2-IRES-Cre mice, or injected AAV5-Syn-ChR2-mCherry bilaterally into the VTA of ePet1-Cre mice at the following coordinates: anteroposterior (AP): −3.0 mm, mediolateral (ML): ± 0.40 mm, dorsoventral (DV): −4.35 mm (rostral); AP: −3.6 mm, ML: ± 0.40 mm, DV: −4.40 mm (caudal). To express opsins in the DRN, we injected AAV5-ef1a-DIO-ChR2-mCherry unilaterally into the DRN of Gad2-IRES-Cre or ePet1-Cre mice at the following coordinates: AP: λ −0.6 mm (bregma −4.8), ML: 0 mm, DV: −3.0 mm, 10° angle from coronal. The viruses were diluted to 3×10^{12} gc/ml with phosphate-buffered saline (PBS) before use and injected with 100 nL per injection site into the VTA (total volume 200 nl) and with 150 nL into the DRN (total volume 150 nl). Mice were used for subsequent experiments 4–6 weeks after AAV infection.

Rabies virus-mediated retrograde and transmonosynaptic tracing from the DRN were used to examine the connections between the DRN and VTA. AAV9-CAG-DIO-GFP-TVA and AAV9-CAG-DIO-RVG (diluted to 3×10^{12} gc/ml before use, volume ratio: 1:1, total volume of 150 nl) were injected into the DRN region of Gad2-IRES-Cre and ePet1-Cre mice at the following coordinates: AP: λ −0.6 mm (bregma −4.8), ML: 0 mm, DV: −3.0 mm, 10° angle from coronal. Two weeks later, RV-EnVA-dsRed (titer, 2×10^{8} colony forming units (cfu)/ml; volume, 200 nl) was injected into the DRN at the same location. Mice were sacrificed 7 d after rabies virus

infection. Only neurons expressing both RVG and EnvA cognate receptor TVA allowed retrograde spreading of the rabies virus to presynaptic neurons. Neurons that expressed both GFP (from helper virus) and dsRed (from rabies virus) were defined as starter cells, whereas neurons that expressed only dsRed were their presynaptic partners and defined as input cells in this study.

Rabies tracing control experiments were performed to verify the specificity of the system. To test for the leakiness of the system, AAV9-CAG-DIO-GFP-TVA and AAV9-CAG-DIO-RVG were injected into the DRN of wild-type mice, followed by RV-EnVA-dsRed in the same place after two weeks. Mice were sacrificed one week later, and locally infected neurons expressing dsRed in the DRN and long-distance labeled neurons in the VTA were calculated. To evaluate if the rabies virus could retrogradely and transmonosynaptically infect neurons in the absence of the RVG protein, we injected AAV9-CAG-DIO-GFP-TVA but not AAV9-CAG-DIO-RVG into the DRN of Gad2-IRES-Cre and ePet1-Cre mice, followed by RV-EnVA-dsRed in the same place after two weeks. Mice were sacrificed one week later, and locally infected neurons expressing both GFP and dsRed in the DRN and long-distance labeled neurons in the VTA were calculated.

Histology and imaging

Mice were deeply anesthetized and transcardially perfused with 0.9% saline followed by 4% paraformaldehyde (PFA) in PBS (pH 7.4). Brains were carefully removed and post-fixed with 4% PFA for an additional 4–6 h. Next, brains were transferred to 30% sucrose dissolved in PBS until they sank to the bottom of the container and were then sliced into 50-μm coronal sections using a freezing microtome (Leica, CM3050 S, Germany). The sections were stored at −20°C in a solution that contained 30% glycerol (v/v), 20% ethylene glycol (v/v), and PBS until they were processed.

For immunofluorescence staining, free-floating sections were washed with PBS three times (5 min each) and incubated with blocking buffer that contained 5% goat serum and 3% bovine serum albumin (BSA) dissolved in 0.5% PBST (0.5% Triton X-100 in PBS) for 1 h. Sections were then incubated with primary antibodies diluted in blocking buffer overnight at 4°C. After incubation, the sections were rinsed four times (15 min each) with PBS and incubated with a fluorescent dye-conjugated secondary antibody (1:400, Invitrogen or Jackson ImmunoResearch, USA) for 2 h at room temperature. Following four washes (15 min each time) with PBS, sections were incubated with DAPI (1:1000, Invitrogen, USA) for 5 min, again washed several times, and then mounted under coverslips with Fluoromount aqueous mounting medium (Sigma-Aldrich, USA). In biocytin-injected slices, Alexa Fluor 633-conjugated streptavidin (1:1000, Invitrogen, USA) was added to the secondary antibody solution. Primary antibodies were: anti-$GABA_AR$ α1 subunit (1:1000, rabbit, Millipore, USA), anti-TH (1:400, mouse, Immunostar, USA), anti-MOP (1:500, guinea pig, Millipore, USA), and anti-Tph2 (1:800, rabbit, Novus Biologicals, USA).

Placement of the cannula was assessed based on lesions in the tissues produced by cannula tips. The expressions of virus-infected cell bodies and axons were outlined on corresponding sections according to the Mouse Brain in Stereotaxic Coordinates (Paxinos and Franklin, 2013). The outlined areas were overlaid at 10%–20% transparency for each mouse to visualize the center of virus and axon expression. For quantification of starter and input cells in the rabies tracing experiment, three sections around the DRN, rVTA, and cVTA were counted manually using NIH ImageJ software. The sections used were at the same coordinates among each group.

Whole slides were imaged at 10 × objective on an Olympus VS120 virtual slide microscope system. Other images were obtained with a Nikon A1 confocal microscope at 10 ×, 20 ×, or 60 × objective, and processed with NIH ImageJ software.

Acute brain slice preparation

Eight- to ten-week-old mice were deeply anesthetized and perfused with ice-cold oxygenated (95% O_2 and 5% CO_2) cutting ACSF consisting of (in mM): 110 choline chloride, 2.5 KCl, 1.3 NaH_2PO_4, 25 $NaHCO_3$, 0.5 $CaCl_2$, 7 $MgCl_2$, 20 glucose, 1.3 Na-ascorbate, and 0.6 Na-pyruvate. Brains were removed quickly, and 250-μm thick coronal slices of the DRN were prepared with a vibratome (Leica, VT1200, Germany) in the cutting ACSF. The slices were recovered for 25–30 min at 34°C in oxygenated incubating ACSF containing (in mM): 125 NaCl, 2.5 KCl, 1.3 NaH_2PO_4, 25 $NaHCO_3$, 2 $CaCl_2$, 1.3 $MgCl_2$, 10 glucose, 1.3 Na-ascorbate, 0.6 Na-pyruvate, and 0.0025 L-Try, and then maintained at room temperature.

In vitro electrophysiology

For recordings, slices were transferred to a recording chamber perfused with recording ACSF containing (in mM): 125 NaCl, 2.5 KCl, 1.3 NaH_2PO_4, 25 $NaHCO_3$, 2 $CaCl_2$, 1.3 $MgCl_2$, and 11 glucose saturated with 95% O_2 and 5% CO_2. Whole-cell patch-clamp recordings were performed at room temperature with a MultiClamp 700B amplifier (2 kHz low-pass filtered, 10 kHz digitization, Molecular Devices, USA) and a 1440A interface (Molecular Devices, USA) with pClamp 10.4 software (Molecular Devices, USA). Fluorescent cells were visualized under a Nikon Eclipse FN1 microscope equipped with a 40 × water-immersion lens and illuminated with a mercury lamp. Whole-cell patch-clamp recordings were used unless other claimed. Data were collected 2 min after obtaining a stable whole cell configuration.

In Figures 2, S3M–S3P, and S4A–S4C, voltage-clamp mode was used for eIPSC recordings (holding potential, −70 mV) with electrodes (3–5 MΩ) filled with an internal solution containing (in mM): 110 potassium gluconate, 40 KCl, 10 HEPES, 3 Mg-ATP, 0.5 Na_3-GTP, 0.2 EGTA, and 0.2% biocytin (pH 7.3) (Pan et al., 2015). We bath applied PTX (50 μM, Tocris, UK) to block $GABA_AR$-mediated IPSCs. Both TTX (1 μM, Tocris, UK) and 4-AP (100 μM, Sigma-Aldrich, USA) were used, as described in the main text.

In Figure 3, current-clamp mode was used to record the firing rates of GABAergic and non-GABAergic neurons. The internal solution consisted of (in mM): 140 potassium gluconate, 5 KCl, 10 HEPES, 2 $MgCl_2$, 4 Mg-ATP, 0.3 Na_3-GTP, 0.2 EGTA, and 10 Na_2-phosphocreatine (pH 7.3). The baseline membrane potential was held at −45 mV to induce action potentials (reverse potential of Cl^- is around −70 mV). The neurons were recorded for 3 s as the baseline, followed by 3 s of light stimulation, and 3 s of recovery, with five repeated sweeps in the presence of DNQX (20 μM, Tocris, UK) and AP-V (50 μM, Tocris, UK). The firing rates during the three epochs in the five sweeps were calculated. The same internal solution was used in Figures S3E and S3F and S4D–S4F. In Figures 3I–3L voltage-clamp mode was used to record the spontaneous firing of DRN serotonergic neurons by cell attached recording in the presence of NE (30 μM, Sigma, USA), DNQX (20 μM, Tocris, UK), and AP-V (50 μM, Tocris, UK) in bath solution, with the internal solution consistent with the recording buffer.

The sIPSCs in Figures 3 and 6 and eIPSCs in Figures 5, 6, and S7 were recorded in voltage-clamp mode (holding potential, −70 mV) in the presence of DNQX (20 μM, Tocris) and AP-V (50 μM, Tocris) in bath solution. The internal solution consisted of (in mM): 130 CsCl, 5 NaCl, 10 TEA, 10 HEPES, 3 Mg-ATP, 0.5 Na_3-GTP, and 0.2 EGTA (pH 7.3). For the strontium-mediated qIPSC measures in Figures S7A–S7D, Ca^{2+} was replaced by the same amount of Sr^{2+} in the recording ACSF to induce asynchronous release. The frequencies and amplitudes were evaluated 10–60 ms after light initiation. The amplitude of each event was measured from a local baseline just before the event.

Photostimulation (473 nm, ~2 mW, 5-ms pulses; 589 nm, ~2 mW, 1 s) was delivered through an optical fiber (200-μm diameter, NA 0.22, Inper, Hangzhou, China) placed near the slice connected to a solid-state laser. A Polygon Patterned Illuminator (Mightex, Polygon400, USA) was used to deliver different intensities of blue light through the 40 × objective to generate the input-output curve in Figure 6I. Slices were fixed with 4% PFA in PBS for immunohistochemical staining after recording if needed. Data were measured using Clampfit 10.4 and Mini Analysis software.

In vivo local field potential recordings

Mice were deeply anesthetized with isoflurane and placed in a stereotaxic apparatus (RWD, 68030, 68025, Shenzhen, China). Optical fibers (200 μm diameter, NA 0.22, Inper, Hangzhou, China) and electrodes (1 Ω, A-M System, USA) were bound together and placed in the VTA or DRN to record local neuronal responses to photostimulation. Local field potentials were digitized at 1 MHz and filtered between 10 Hz and 100 Hz. Extracellular spikes were digitized at 1 MHz and filtered between 300 Hz and 3 kHz. An 1800 amplifier (A-M System, USA) and 1440 A interface (Molecular Devices, USA) were used to record electrophysiological signals *in vivo*.

Real-time place preference/aversion

On day 1, mice were placed in a Plexiglas box with two connected chambers (25 cm × 25 cm × 50 cm each chamber) and allowed to freely explore for 15 min. One chamber was randomly designated as the stimulation chamber, and the other was designated as the non-stimulation chamber. The percentage of time spent in the stimulation chamber was measured as the baseline, and mice with a bias for one side were excluded. On day 2, mice were randomly placed in either chamber and received 20-Hz blue light pulses or sustained yellow light each time they entered the stimulation chamber until they entered the non-stimulation chamber. Time spent in each chamber was measured every 10 min for 30 min. Travel traces and time spent in each chamber were recorded by the ANY-maze behavioral recording system.

Open field test

Mice were placed in an open field arena (50 cm × 50 cm × 50 cm) and allowed to freely explore for 8 min. A 20-Hz photostimulation was delivered during the 3rd to 4th and 7th to 8th minutes. Total distance traveled was recorded by a MED behavioral recording system.

Elevated plus maze test

The maze consisted of four crossing arms (two open and two closed) placed at a height of 50 cm above the ground. Mice were placed in the center of the platform at the beginning of the experiment and allowed to freely explore the maze for 8 min. A 20-Hz, 5-ms photostimulation was delivered during the 3rd to 4th and 7th to 8th minutes. Locations of mice were tracked with the MED behavioral recording system.

Morphine-induced locomotor, CPP, and withdrawal

A three-chamber apparatus was used in the CPP experiments. Two chambers (20 cm × 20 cm × 50 cm each chamber) were distinguished by different wall colors (black and white) and floor patterns (bar type and holes) and separated by a corridor (10 cm × 20 cm × 50 cm). A video tracking system was used to record mouse movements. On day 0, mice freely explored the apparatus for 30 min to record time spent in the white chamber. Six hours later, mice were placed in the white chamber for 1 h to test total distance traveled as the baseline for locomotor activity. The conditioning session was conducted from day 1 to 5, with the white chamber associated with intraperitoneal injection of morphine at increasing doses (10, 20, 30, 40, 50, 50 mg/kg) for 1 h, then 6 h later, the black chamber was associated with saline injections at the same volumes for 1 h. The mice were microinjected with CNO into the DRN 5 min before morphine administration. Total distance traveled in the white chamber was recorded. Day 6 was the test session, with mice allowed to freely explore the whole apparatus for 30 min to record time spent in the white chamber. The CPP score was measured as time spent in the white chamber on day 6 subtracted by time spent in the white chamber on day 0. Mice were placed into their home

cages and injected with morphine 30 min after the test. Two hours later, the mice were injected with naloxone (5 mg/kg) to induce withdrawal behaviors. Rearing number was recorded for the next 20 min in the home cage and counted offline as a physical sign of withdrawal.

Tail flick test

The tail flick test was used to measure the analgesic effects of morphine and tolerance induced by repeated morphine administration. Mice were restrained and the tips of their tails (about 2–3 cm) were immersed into 50°C hot water. The mice will withdraw their tails as they feel pain. The latency for the mouse to lift its tail from hot water was noted as tail flick latency. To prevent tissue damage, the test was terminated if the mouse failed to lift its tail within 30 s. One day 0, tail flick latency was tested as the baseline. Mice then underwent 5 d of repeated morphine treatment at the same dose (15 mg/kg) and time each day. On day 1, tail flick latency was measured 40 min after morphine treatment to assess the analgesic effects of morphine. On day 5, tail flick latency was measured 40 min after morphine treatment to assess tolerance induced by repeated morphine exposure.

Cannula implantation and *in vivo* opto-stimulation

For *in vivo* optogenetic manipulation, optical fiber cannulas (200-μm diameter, RWD, Shenzhen, China) or ferrules (200-μm diameter, NA 0.22, Inper, Hangzhou, China) were implanted into the DRN (AP, −4.8 mm; ML, 0 mm; DV, −2.8 mm, 10° angle from coronal) of mice 3–5 weeks after virus injection. Mice were allowed to recover for at least one week after implantation. Mice were habituated for 30 min after connection to a laser source or application of a drug through the cannula, after which behavioral tests were performed. Lasers at wavelengths of 473 nm (blue) or 589 nm (yellow) were applied and controlled with an intelligent optogenetic system (Inper, Aurora-200, Hangzhou, China) at ~2 mW.

In the microinjection experiments, the microinjector was 200 μm longer than the guiding cannula and was attached to a polyethylene tube connected to a 1 μL Hamilton syringe (Hamilton, Nevada, USA) at the other end. Drugs were infused into the DRN by hand over 2–3 min. The microinjector was left in the DRN for a further 1 min to allow the drug to diffuse. We used 0.3 mM × 300 nL picrotoxin dissolved in ACSF, and 3 μM × 150 nL of CNO dissolved in ACSF for the experiments. Mice were placed in the experimental apparatus 5 min after microinjection or connected to the optical fibers immediately.

QUANTIFICATION AND STATISTICAL ANALYSIS

One-way ANOVA, two-way ANOVA, or t-tests were used to analyze data when applicable. Non-parametric tests were used if the data did not meet the assumptions of parametric test. All of the statistical details of experiments can be found in the figure legends. Data were presented as means ± standard errors of the means (s.e.m.). Significance was defined as $p < 0.05$. All data were collected randomly. Sample size were chosen according to previous papers. Statistical analyses were performed with GraphPad Prism 5 or Origin 8 software.